REPORT DOCUMENTATION PAGE

AFRL-SR-BL-TR-98-

0496

Public reporting burden for this collection of information is estimated to average 1 hour per response, in ... sources, gathering and maintaining the data needed, and completing and reviewing the collection of information. ... ect of this collection of information, including suggestions for reducing this burden, to Washington Headquarters S ... Jefferson Davis Highway, Suite 1204, Arlington, VA 22202-4302, and to the Office of Management and Budget, Paperwork ... 3.

1. AGENCY USE ONLY *(Leave blank)*	2. REPORT DATE	3. REPORT TYPE AND DATES COVERED
	May 1998	Final Technical Report 15 Aug 94 to 14 Nov 97

4. TITLE AND SUBTITLE
DEVELOPMENT OF DOPPLER GLOBAL VELOCIMETER (DGV)

5. FUNDING NUMBERS
F49620-94-1-0434

6. AUTHOR(S)
John Kuhlman, PI

7. PERFORMING ORGANIZATION NAME(S) AND ADDRESS(ES)
West Virginia University
Mechanical and Aerospace Engineering Dept
Morgantown, WV 26506-6106

8. PERFORMING ORGANIZATION REPORT NUMBER

9. SPONSORING/MONITORING AGENCY NAME(S) AND ADDRESS(ES)
AFOSR/NA
110 Duncan Avenue, Ste B115
Bolling AFB, DC 20332-8050

10. SPONSORING/MONITORING AGENCY REPORT NUMBER
F49620-94-1-0434

11. SUPPLEMENTARY NOTES

19980617 019

12a. DISTRIBUTION AVAILABILITY STATEMENT
Approved for public release; distribution unlimited.

...N CODE

13. ABSTRACT *(Maximum 200 words)*

A two-component Doppler Global Velocimeter (DGV) and a two-component Point Doppler Velocimeter (PDV) are descried Velocity measurements for both systems to quantify accuracy are presented. Results are presented for velocity distributions over the surface of a rotating wheel and fully-developed turbulent pipe flow.

Accuracy of PDV wheel velocity data is ±1% of full scale, while linearity of a single channel is on the order of ±0.5% (ie, ±0.6 m/sec and ±0.3 m/sec, out of 57 m/sec). Overall accuracy of wheel data matches cell calibration repeatability. PDV pipe flow data show consistent turbulence intensities, and mean velocities agree with pitot probe data. However, a mean velocity offset error is observed.

DGV system accuracy has also been investigated; this system uses four 8-bit Hitachi CCD cameras, and a Matrox Genesis frame grabber board for image acquisition. For rotating wheel results, RMS noise levels are on the order of ±1 m/sec, while total velocity range errors are between ±1-2 m/sec. RMS noise is dominated by camera resolution. Pipe flow mean velocity measurements show reasonable agreement with centerline pitot probe data. The observed zero velocity offset has been corrected through use of a reference tab, to record zero velocity signals.

14. SUBJECT TERMS

15. NUMBER OF PAGES
37

16. PRICE CODE

17. SECURITY CLASSIFICATION OF REPORT	18. SECURITY CLASSIFICATION OF THIS PAGE	19. SECURITY CLASSIFICATION OF ABSTRACT	20. LIMITATION OF ABSTRACT
Unclassified	Unclassified	Unclassified	UL

DEVELOPMENT OF DOPPLER GLOBAL VELOCIMETER (DGV)
Final Report for AFOSR/DEPSCoR Grant F49620-94-1-0434
May 1998

John Kuhlman, PI
West Virginia University
Mechanical and Aerospace Engineering Department
Morgantown, WV 26506-6106

ABSTRACT

The development of a two-component Doppler Global Velocimeter (DGV) system is described, along with a companion two-component Point Doppler Velocimeter (PDV) system. A series of velocity measurements obtained for both systems in order to quantify their accuracy is presented. These DGV and PDV systems use molecular iodine vapor cells as frequency discriminating filters to determine the Doppler shift of laser light which is scattered off of seed particles in a flow, from which the flow velocity is determined. Results are presented for velocity distributions over the surface of a rotating wheel and a fully-developed pipe flow.

Accuracy of the present PDV wheel velocity data is approximately ± 1 % of full scale, while linearity of a single channel is on the order of ± 0.5 % (ie, ± 0.6 m/sec and ± 0.3 m/sec, out of 57 m/sec, respectively). The observed linearity of these results is on the order of the accuracy to which the speed of the rotating wheel has been set for individual data readings. The overall accuracy of the rotating wheel data has been found to be consistent with the level of repeatability of the cell calibrations. The PDV turbulent pipe flow data show consistent turbulence intensity values, and mean axial velocity profiles generally agree with pitot probe data. However, an offset error is observed in the mean velocity which is on the order of 5-10 % of the maximum axial velocity.

The accuracy of the DGV system has also been investigated. This two-component DGV system uses four 8 bit Hitachi CCD cameras, and a Matrox Genesis frame grabber board for image acquisition. Image acquisition software is described, along with the required image processing software, including the required image warping and pixel registration routines, calibration, averaging, and so forth. For the rotating wheel results, RMS noise levels are observed which are on the order of ±1 m/sec, while total velocity range errors are observed to be between ±1-2 m/sec. The RMS noise is dominated by the 8 bit camera resolution. Both of these errors for the DGV measurements are 2 to 3 times larger than those observed for the PDV system. An example fully turbulent pipe flow mean velocity measurement shows reasonably good agreement with centerline pitot probe traverse data. The zero velocity offset that has been observed has been corrected through the use of a reference tab, to record the zero velocity signals in each image.

INTRODUCTION

This research project is exploring the accuracy of Doppler Global Velocimetry (DGV), a nonintrusive, planar imaging, Doppler-based velocimetry technique, as well as the accuracy of related Point Doppler Velocimetry (PDV). Both of these techniques use an iodine vapor cell absorption line filter (ALF) to determine the Doppler shift, and hence the velocity, of small seed particles in a flow field, as these particles pass through a two-dimensional sheet of laser light. The same portion of the light sheet is viewed through a beamsplitter, either by a pair of video cameras (for DGV), or a pair of photodetectors (for PDV), with the iodine cell ALF placed in the optical path of one of the cameras or photodetectors (**Fig. 1**). Laser wavelength and ALF absorption band are matched such that the range of flow velocities of interest yields Doppler shifted frequencies which lie in the linear portion of the absorption band of the ALF. As a result, the ratio of the light intensities seen by the two detectors at a point in the flow yields a signal which is proportional to the particle velocity.

For a non-scanned "point" PDV system, very high data rates are possible, limited primarily by seeding/signal strength and A/D conversion speed. Use of conventional CCD cameras to view a region of the light sheet yields velocity data in a plane at a typical resolution of 640 pixels by 480 lines, at framing rates of up to standard video rates of 30 frames per second, but at a reduced accuracy (typically demonstrated to be on the order of about 5 %). This reduced accuracy is primarily due to camera noise and pixel registration errors, as well as laser speckle noise for systems using pulsed YAG lasers (McKenzie, 1997; Smith and Northam, 1995). Cooled cameras can reduce noise, but at a significant increase in cost and reduction in data rates. Further, these cameras do not reduce noise due to laser speckle. Pixel registration errors are minimized through a series of software corrections.

A two-channel non-scanned point PDV system has been developed in the current project (Kuhlman, et al., 1997). A two-channel scanned DGV system using CCD cameras has also been developed (Naylor and Kuhlman, 1998). The accuracy limits of both systems are being systematically explored, through a series of measurements in relatively simple, unheated flows such as fully-developed turbulent pipe flow and a turbulent circular jet. A rotating wheel is also being used as a velocity standard. The present report describes both the two-channel PDV and DGV systems and the related software, and presents a series of velocity measurements for a rotating wheel and a fully-developed pipe flow, which have been taken to assess the accuracy of both systems for mean and RMS velocity measurements.

LITERATURE SUMMARY

Several different non-intrusive whole field velocimetry techniques are currently under development which provide velocity data in a plane, which can thus greatly reduce the time required to map out a complex flow field. It is expected that this can lead to enhanced insight into flow physics, as well as allow investigation of a greater number of flows in parametric studies. Of these techniques, particle image velocimetry (PIV) has perhaps been the most fully developed (Adrian and Yao, 1983). Scalar imaging velocimetry (SIV) shows promise for determination of three dimensional velocity data in large Schmidt number liquid flows (Dahm, 1992). Another nonintrusive technique under development by Miles (1992) is the RELIEF technique, which also appears to be limited to two velocity components in a plane, similar to PIV.

A fourth concept for acquiring non-intrusive real-time velocity measurements in a planar region called Doppler global velocimetry (DGV) has been patented by Komine (1990). This technique uses a pair of video cameras and an iodine vapor cell absorption line filter (ALF) for each velocity component, to measure the average Doppler frequency shift, averaged over each pixel, of the light scattered off minute seed particles in a flow as they pass through a planar sheet of laser light. A group at the NASA Langley Research Center (Meyers et al., 1991) is currently developing this new DGV velocity measurement technique into an accurate instrument. This same group has also funded work at Northrop (Meyers and Komine, 1991).

Others are also developing concepts similar to DGV; for example, Miles, et al. (1991) have developed a filtered Rayleigh scattering (FRS) technique which allows nonintrusive velocity measurements without requiring any seeding. An optically thick ALF is used to filter out all signal but the Doppler shifted frequencies due to molecular Rayleigh scattering. Accuracy of this technique in supersonic flows has been documented in Forkey, et al. (1995) to be comparable to that of DGV, on a percentage basis.

Hoffenberg and Sullivan (1993) have measured the velocity of a jet at a point, using a non-scanned filtered particle scattering (FPS) technique. Accuracy of both mean and turbulence quantities for this point system was comparable to LV data near the centerline at the exit of an axisymmetric jet at about 100 ft/sec. However, large errors in mean and RMS velocities were found near the edges of the jet, possibly due to uneven seeding and low signal-to-noise ratio. Similar point PDV studies have been conducted by Morrison, et al. (1994), and by Roehle and Schodl (1994). Roehle and Schodl have improved the accuracy of their measurements through active stabilization of the frequency of their CW Argon ion laser.

More recently, others at NASA Ames (McKenzie, 1995, 1997), NASA Langley (Smith and Northam, 1995), and Ohio State University (Elliott, et al, 1994, and Clancy and Samimy, 1997) have also developed scanned DGV systems. Smith, McKenzie, and Clancy and Samimy each have used a single video camera to record both the reference and signal images for each velocity component; this split-image technique reduces resolution by a factor of two, but also reduces system cost and complexity. The data by McKenzie for single channel point measurements on a rotating wheel (1995) display an absolute accuracy on the order of ± 1-2 m/sec. McKenzie's more recent (1997) planar imaging results of the velocity of the same rotating wheel displayed a lower level of accuracy (±2-5 m/sec). The present two-component PDV results by Kuhlman, et al. (1997), for a rotating wheel displayed an accuracy on the order of ± 0.5-1 m/sec. Irani, and Irani and Miller (1995) have investigated the accuracy of a single-component DGV system. Recently, Elliott, et al. (1997) have presented DGV results for transverse jet injection into a supersonic free stream. Beutner and Baust (1997) have given details of a DGV system which is under development at the Wright Laboratory. Reinath (1997) has given a detailed description of a three-component DGV system that has been developed for use in wind tunnels at the NASA Ames Research Center.

Thus, it is clear that in a very short time (approximately seven years), DGV has developed to a point where capability has been demonstrated for making non-intrusive mean flow velocity vector measurements in a plane, in a variety of complex single phase flow fields of practical significance. While current scanned DGV systems lack the accuracy or resolution of conventional LV systems or PIV (to date, documented as on the order of 5 %, versus 1 % for LV, at about 100 ft/sec.), DGV has proven in a very short time to be an extremely flexible whole-field velocimetry technique.

Following the notation of McKenzie (1995), the basic equation relating the Doppler shift frequency to the resolved velocity component is given by

$$\delta\upsilon = \frac{(\mathbf{a}-\mathbf{l})\bullet\mathbf{V}}{\lambda} \tag{1}$$

where $\delta\upsilon$ is the Doppler frequency, **V** is the velocity vector, λ is the incident laser frequency, and **a** and **l** are the observer and laser propagation directions, respectively. Thus, the resolved velocity component is in the direction of the sum of **a** and (-**l**); see **Fig. 2**. Viewing the light sheet from three different directions enables determination of the three dimensional velocity field in a plane.

APPARATUS AND PROCEDURE FOR PDV SYSTEM

The present point PDV system closely follows the basic DGV configuration using two inch diameter iodine cells which was originally developed by Meyers et al. (1991), except that photodiodes are currently being used, along with front lenses and pinholes, to collect scattered light from a single point in a seeded flow which is illuminated by a CW Argon ion laser. Laser frequency has not been actively controlled, but instead a reference iodine cell has been used to compensate for any changes (due to laser frequency drift) in the voltage ratios for the iodine cells which view the flow and receive the Doppler shifted scattered light. A laser spectrum analyzer has been used to monitor laser mode shape and detect the occurrence of mode hops. After a suitable warm-up period for the laser and spectrum analyzer (typically on the order of one hour, to achieve optimum frequency stability), frequency drift on the order of 50 MHz has been observed over a time period on the order of 30 minutes; this is close to the resolution of the spectrum analyzer and the claimed frequency stability for the laser.

This reference iodine cell system and the Argon ion laser are shown in **Fig. 3**, along with the laser spectrum analyzer and Argon ion laser. Neutral density filters and a beam expander are used to ensure that the iodine cell is not saturated by the reference beam. The layout of one of the two PDV channels is shown in **Fig. 4**, while a schematic of how the entire system has been configured for the wheel velocity measurements may be found in **Fig. 5**. The two PDV channels include pinholes behind each front lens, as implemented by Roehle and Schodl (1994); these pinholes act as spatial filters to set the size of the sensing region in the light sheet, as well as to reduce the effects of secondary scattering by limiting the depth of field. Plano-convex lenses have been installed in front of the photodiodes (see **Fig. 4**), to ensure that all scattered light from the sensing region is imaged onto the photodetectors. Also, improvements in accuracy have been obtained by carefully optimizing and matching amplifier gains for each pair of photodiodes, as well as by enclosing each PDV channel to reduce background scattered light intensities.

Achieving adequate temperature stability of the side arms of the iodine cells has been found by researchers at NASA Langley to be an essential requirement for accurate operation of a DGV system. A temperature control system which is similar to those used by NASA Langley has been implemented in the present system, which is comprised of a pair of electrical band heaters which heat a hollow bushing made from oxygen-free copper, which surrounds the iodine cell except for the two optical windows and the side arm. The side arm has been thermally "grounded" by a copper wire which is bonded to the tip of the side arm, and then bolted to the optical breadboard on which the DGV system is mounted. The entire system has been enclosed in an insulated box (as shown in exploded view in **Fig. 4**) to shield the cell from air currents or room temperature variations, and the optical windows of the cell have been insulated from the room air by phenolic tubes fitted with additional AR-coated crown glass windows, which protrude through the sides of the aluminum box. This creates a heated dead air space next to the outside of the cell by the optical windows and prevents the formation of solid iodine crystals on the optical windows. The Omega PID temperature controller has been adjusted to achieve very stable operation, where the copper sheath surrounding the iodine cell typically operates at a temperature that is nominally 10°C above the side arm temperature. This ensures that all solid phase iodine collects in the side arm of the cell. Cells have been operated at stem temperatures of 45°C, since absorption well slope is a maximum there (McKenzie, 1995).

Data acquisition software has been developed in Visual Basic 4.0 to allow continuous monitoring and data acquisition of the cell temperatures, for the reference cell and each of the cells used in the two PDV channels. Long term drift in iodine cell temperature has been measured to be on the order of ± 0.1°C (the specified set point accuracy of the temperature controller), once the cell has warmed up to its steady operating temperature. Short term fluctuations have been measured which are on the order of 0.03-0.04 °C; this approaches the resolution of the 16 bit thermocouple A/D board.

To determine the accuracy of the two-component PDV system, a rotating wheel apparatus has been developed, consisting of a 12 inch diameter, anodized circular aluminum disk which has been painted white, and mounted on a variable speed DC motor. This wheel can achieve tip velocities of approximately ± 29 m/sec. In addition, a calibration procedure similar to that which has been used by NASA Langley personnel, where the laser is mechanically mode hopped by tilting the etalon has been utilized to calibrate the iodine cells.

A 1.5 inch diameter, fully-developed turbulent pipe flow apparatus has been developed, as has a small grid turbulence flow facility. Also, a jet facility is available which has interchangeable convergent nozzles with exit diameters of 0.375, 0.5, and 1.0 inches, and which can attain exit velocities up to 120 m/sec, with very low exit turbulence levels. Kuhlman (1994) has given a conventional LV data set for this jet, as well as for a companion annular jet. Flow seeding has been achieved using a commercial fog machine in the present work.

A computer-controlled, three-axis traversing system has been developed (**Fig. 6**), as described in the thesis by Ramanath (1997), for use in positioning the flow facilities with respect to the fixed, two channel PDV system, so that velocity contours may be mapped out in a plane or volume. This traverse allows movement in a volume which is two feet by a foot and a half in a horizontal plane, by one foot in the vertical direction. Accuracy of a single traverse move has been found to be better than 0.001" for typical moves on the order of a few inches (Ramanath, 1997).

An 8 channel, 16 bit, simultaneous-sample-and-hold IOTech A/D board is used for digital data acquisition of the photodetector output voltages for the reference iodine cell, and for the two PDV channels. The RMS noise level for this board is ± 0.3 mV on a 10 volt scale. Windows-based data acquisition software has been developed (again, using Visual Basic) for this board. In addition, companion VB data reduction programs have been developed, to automate the data reduction process.

Calibration of the iodine cells has been accomplished using a continuous scan of the mode structure of the Argon ion laser, by mechanically altering the tilt of the etalon through about 10-20 mode hops, over a 20-30 second period. A typical time history of the voltage ratios for the reference channel and the two signal channels for this process is shown in **Fig. 7**. It is generally noted that the signal-to-reference voltage ratio for each iodine cell varies continuously between mode hops. Occurrence of mode hops has been detected by a sudden jump in reference photodiode voltage. The ratio value for any one mode hop may be computed as an average value, the value at the left end of that mode, or the value at the right end of the mode; the best results have been obtained using the average value (James, 1997). It has been found that this continuous scan mode hop calibration technique offers better accuracy than an earlier technique, where individual ratio values were measured after each mode hop of the laser. This is because the cell temperatures cannot change significantly over the 20-30 second time period required to perform a scan. Also, the effects due to variability of where one stops the mechanical screw adjust on the etalon tilt screw are minimized by this technique. Significant further improvement in calibration accuracy has also been obtained by averaging several of these individual continuous scan mode hop calibrations together. This improved calibration consists of several (from 3 to 6) continuous mode hop calibration data sets for each cell. A single cell calibration data file is formed by "sliding" all mode hop calibrations for any one cell, to overlay them on one arbitrarily-selected calibration of the set. This procedure is accomplished by linear interpolation, and is necessary because of laser drift between mode hop calibrations, where the ratio value for the n^{th} mode hop for any one cell will change, especially when the room temperature varies significantly.

APPARATUS FOR DGV SYSTEM

The present DGV system also closely follows the basic DGV configuration using two inch diameter iodine cells which was originally developed by Meyers, et al. (1991). DGV system hardware and software (see next section) have been described previously in Naylor and Kuhlman (1998). Most of this hardware is similar to that used for the PDV system, as has been described above. The identical reference iodine cell system, laser, and spectrum analyzer, shown in **Fig. 3** for the PDV system, has been used for the DGV system. The same data acquisition software has been used to monitor the cell stem and body temperatures, for the reference cell and each of the cells used in the two DGV channels.

The same rotating wheel apparatus has been used to determine the accuracy of the two-component DGV system, along with the same 1.5 inch diameter, fully-developed turbulent pipe flow apparatus (shown in **Fig. 6**) which was used for the PDV system. Flow seeding for DGV measurements is provided by a commercial fog machine, which feeds a large plenum, to damp out pulsations in smoke output. This has led to better uniformity in the signal levels from image to image for the pipe and jet flow data.

The computer-controlled, three-axis traversing system (**Fig. 6**) has been used for positioning the flow facilities with respect to the fixed, two channel DGV system, so that pipe and jet flow velocity contours may be mapped out in several planes. The 8 channel, 16 bit, simultaneous sample-and-hold IOTech A/D board has been used for digital data acquisition of the photodiode output voltages for the reference iodine cell.

Eight bit Hitachi KP-M1 CCD cameras and a Matrox Genesis frame grabber have been used for the two-component DGV system. The frame grabber has four inputs, each leading to eight bit digitizers. This configuration allows all four cameras to be read simultaneously, as long as the cameras have been synchronized. The same horizontal and vertical sync signals are fed to each of the cameras by the Genesis board. Maximizing data rates for this system is not a concern since the fastest data rates possible with the cameras are still not fast enough to resolve any significant time varying flow structures. The continuous data acquisition rate, writing to the hard drive, for the two-component system is approximately 2 sets of four frames/sec, while short bursts of data (10 frames total from each camera) may be acquired at 30 frames/sec, by using the on-board memory of the Genesis board.

Fig. 1 shows a top view photo of one of two DGV channels. Attached to the front of the cameras are Nikon 35-135mm, f 3.5-4 zoom lenses mounted on C-mount adapters. Zoom lenses were selected instead of fixed focal length lenses because of their versatility in imaging different sized areas over a wide range of distances. The penalty paid for this flexibility is an increased f-number for a given focal length relative to a fixed focal length lens. This both decreases the amount of incoming light and increases somewhat the noise due to laser speckle (McKenzie, 1997; Smith and Northam, 1995). Polarizing filters have been placed in front of the beam splitters to minimize effects due to polarization sensitivity of the beam splitters.

DATA ACQUISITION AND IMAGE PROCESSING FOR DGV SYSTEM

Introduction

The software written for both image processing and the operation of the frame grabber is a mixture of C and Visual Basic. VB provides the front-end for all grabbing and processing DLLs, which have been written in C. The acquisition hardware for the reference (photodiode) system is housed in one personal computer, while the frame grabber is installed in a different, but nearby, PC. The problem of synchronizing the photodiode and camera based acquisitions for both calibration and velocity data has been solved through the use of digital inputs and outputs on both systems. Handshaking ensures that both systems are ready before any triggering is enabled. When the signal is given to start data acquisition, the frame grabber simultaneously grabs one field (half of a full image--due to interlacing) for each camera, while the A/D board samples the reference photodiodes for the same $1/60^{th}$ of a second. Because one field is taken after another, $1/60^{th}$ of a second apart, the two fields that make up an interlaced image cannot be used as one velocity image in DGV. In post-processing, the missing lines in the acquired field are filled in using the average of the pixel values directly above and below the empty line, creating a full frame to be analyzed.

Iodine Cell Calibration

Calibration of the iodine cells has again been accomplished using a continuous scan of the mode structure of the Argon ion laser, by mechanically altering the tilt of the etalon through about 10-20 mode hops, over a 20-30 second period. It is generally noted that the signal-to-reference ratio for each iodine cell varies somewhat between mode hops. Occurrence of mode hops has been detected by a sudden jump in reference photodiode voltage. It has been found that this continuous scan mode hop calibration technique offers better accuracy than an earlier technique, where individual ratio values were measured after each mode hop of the laser. This is because the cell temperatures cannot change significantly over the 20-30 second time period required to perform a scan. Also, the effects due to variability of where one stops the mechanical screw adjust on the etalon tilt screw are minimized by this technique.

Significant further improvement in calibration accuracy has also been obtained by averaging several of these individual continuous scan mode hop calibrations together (James, 1997). This improved calibration consists of several (from 7 to 10) continuous mode hop calibration data sets for each cell. A single cell calibration data file is formed by "sliding" all mode hop calibrations for any one cell, to overlay them on one arbitrarily-selected calibration scan of the set. This procedure is accomplished by linear interpolation, and is necessary because of laser drift between mode hop calibrations, where the ratio value for the n^{th} mode hop for any one cell will change, especially when the room temperature varies significantly. After the calibration data is shifted, a best-fit curve is found in order to determine a relative frequency given a measured ratio. The method of fit can presently be one of three choices; a form of a Boltzmann fitting function, an n^{th} order polynomial, or a stretched and shifted curve generated by theoretical means (McKenzie, 1995). Thus far, the latter two have been largely untested for the DGV system. However, on the PDV system, the method that gave the most consistent results was the Boltzmann function (James, 1997).

The form of the Boltzmann fitting function used is as follows:

$$y = \frac{A_1 - A_2}{1 + e^{\left(\frac{x - x_0}{D_x} + A_2\right)}} \tag{2}$$

where A_1 and A_2 are the top and bottom boundary ratio levels, respectively, x_0 is a horizontal frequency shift, and D_x is a horizontal stretching coefficient. This function is heavily used in some neural network algorithms as an activation function. A sample of this curve fit, shown with calibration data for each of the three iodine cells can be seen in **Fig. 8**. Individual data points show less scatter than McKenzie has shown for calibration using a pulsed YAG laser (1997), but there appears to be room for improvement in the curve fitting function shape near the top and bottom of the curves; the present velocity results have been acquired near the middle of these curves.

For the DGV system, the calibration procedure has an added step for the cells that are calibrated with video cameras as opposed to photodiodes. As in the point system, voltage data from the reference system photodiodes is acquired continuously while the laser is mode hopped through an iodine absorption line, but images through the other two cells are acquired as quickly as possible (~2 images/sec). Then, the average gray level within a user-defined area for each calibration image is found and recorded before further data shifting and curve fitting can take place. In this way, the cameras operate as very large, slow, photodiodes.

A typical calibration scan takes up to 30 seconds to complete, while a set of 10 scans can be acquired in 10 to 20 minutes, depending on the behavior of the laser during the scans (scans for which double mode hops have occurred are discarded and repeated). Therefore, cell stem temperature drift is not as much a factor over the course of a single scan as it is during the acquisition of an entire calibration set. Over the course of a single scan, the frame grabber grabs images at a rate that allows 3 or 4 images per mode, whereas the A/D board acquires approximately 100 data points during a single mode for the reference cell. Consequently, after averaging over a mode, data from the cameras is less consistent than that from the photodiodes. Use of a larger number of individual scans in the curve fit process helps to compensate for this variability.

Image Processing Software

The main goal of the image processing software is to more accurately represent the imaged area by better aligning the views of the signal and reference cameras. A block diagram of the data reduction process is shown in **Fig. 9**. Most of the steps shown closely follow the comprehensive image processing methods developed at NASA Langley by Meyers (1992, 1996). Besides the cell calibrations, several additional images need to be taken before each data run, while the system remains undisturbed. In each case where the target is stationary, several exposures are taken and averaged for each camera. The first of these additional images is the background image. The background image is an image (average of several frames) of the data area without laser illumination, which is subtracted from all data images subsequently taken.

The next averaged image is one of a rectangular reference grid of small dots placed in the plane of measurement which is key to the spatial corrections needed for accurate alignment of the signal and reference camera images. This "dot card" image provides reference points with which dewarping calculations are made. The details of the dewarping algorithm will be discussed later, as it is a fairly complex element of the spatial correction process.

An averaged image of a laser-illuminated white card is also recorded. Laser light is used, rather than white light, in an attempt to closely emulate test conditions. Also, the laser is tuned such that the frequency does not fall in an iodine absorption line during this acquisition (McKenzie, 1997). The signal and reference images of the white card go through the same processing steps as do the data images up to the ratio step. After the division of signal and reference images, each channel's white card ratio array is normalized with respect to the average ratio value. The resulting matrix of floating point numbers should, ideally, be equal to 1.0, but spatial imperfections in the imaging system (lenses, beamsplitters, mirrors, and cell ends) will cause variations in the ratio. Ratioed data images are then divided by the white card matrix to correct for these imperfections (Meyers, 1996).

White card images do nothing, however, to account for the slight variations in sensitivity for individual pixels across the CCD array. In an effort to force all pixels in an array to have the same sensitivity, two average images are taken with all lenses removed and the array exposed to two different light levels. These images only need to be taken once, since the pixel sensitivity imperfections are inherent to the cameras and are not likely to change with changes to the configuration or alignment of the system. Individual pixel sensitivities (or slopes), which, ideally, should be equal to 1.0, are calculated at each pixel by

$$\mathrm{slope}_{x,y} = \frac{\mathrm{P1}_{x,y} - \mathrm{P2}_{x,y}}{\mathrm{Avg1} - \mathrm{Avg2}} \tag{3}$$

where $P1_{x,y}$ is the gray level value at the x, y pixel location in the first image, and $P2_{x,y}$ is the pixel value at the same location in the second image. Avg1 and Avg2 are the average gray level values for the first and second images, respectively. The correction is applied by dividing the data image from each camera by the corresponding array of pixel slopes (Meyers, 1992). Naylor and Kuhlman (1998) have shown an example of X and Y cuts through the center of a flat-field image from one of the cameras before and after the pixel sensitivity correction has been applied; see **Fig. 10**. The RMS deviation of the X and Y cuts before the correction are 0.9 and 1.6 gray levels. After the correction, they are both reduced to a value of 0.8. When viewing false color images of the pixel correction buffers, unique "hot spot" patterns can be seen for each camera which are identical in shape to features seen in the raw data images, confirming the need for this type of correction.

The next step in the algorithm is to low-pass filter the image resulting from the steps above. A convolution is performed between a flat 5X5 kernel and the image, in effect, blurring it. Low-pass filtering reduces the effects of both the CCD readout noise, as well as any laser speckle noise (McKenzie, 1997). Speckle noise is less of a problem with the CW laser used in this research than with a pulsed laser, but low-pass filtering still improves the quality of the images acquired. As a result of previous testing of the camera/lens combination, the MTF was found to be approximately 3 to 5 pixels wide, so a 5X5 kernel actually causes minimal loss of meaningful spatial variations in velocity.

The need for dewarping is most obvious when trying to overlay velocity images from different DGV channels, to resolve orthogonal velocity components. Resolution of those components necessitates measuring velocity from different directions, resulting in perspective warping. However, even though both signal and reference cameras within a DGV component system are viewing the same area through a beamsplitter, dewarping is also needed for these images to correct for imperfect pixel-to-pixel alignment (Meyers, 1992). The dewarping process begins with the acquisition of a dot card image by each camera, as described above, which provides an array of discrete reference points with which to align the images. Each dot card image is then masked by thresholding the result of a standard edge-finding (Sobel) filter, and the dot center locations are found using blob centroid analysis techniques, and stored. Next, a grid is generated which marks the location of the dots in the dewarped image. The numbers of rows and columns of dots visible in the distorted image are counted, and the grid coordinates are calculated in such a way as to fill the entire dewarped image with that number of equally spaced points. This has been done so that the warped image is always stretched when dewarped, and pixels referenced in the warped image are guaranteed to be defined within the image area. However, note that the resulting dewarped images thus can have slightly different X and Y scale factors; this distortion has been largely avoided in the present work by using dot cards with the same 4:3 aspect ratio as the camera CCD arrays. Next, the X and Y coordinates of the dewarped image that correspond to locations in the warped (dot card) image are found by ratioing the distances to the nearest dots and equating the ratios in both the warped and dewarped images (Wolberg, 1990). When this is done, there exist two floating point arrays for each camera; one containing X pixel coordinates, the other Y. These floating point numbers represent pixel locations in the warped image, so that bilinear interpolation is performed on each pixel to yield the target gray level value in the dewarped image.

The accuracy of the present dewarping routines has been tested by recording two sets of dot card images, the second of which was translated both horizontally and vertically through a distance equal to one half of the dot spacing. The first set of dot card images was processed as described above to compute the dewarping coefficients, which were then applied to the computed dot card centroid coordinates for the second set of images. If the dewarping process were without error, then the horizontal (X) distances and the vertical (Y) distances which each dot centroid moved in the dewarped images would be the same. For this data set, the computed RMS of the X and Y distances that each centroid moved was approximately 0.1 pixel. Also, the RMS of the difference between computed distances for corresponding dot centroids in the signal and reference camera images for the two DGV channels was approximately 0.2-0.3 pixels. This compares favorably with similar results by McKenzie (1997), where a value of 0.3 pixels has been given. Note that because these results are for positions in the image which are at maximum distances from the image registration locations (the dot centroids of the unshifted images), it is expected that these values are conservative estimates of the level of image overlay that has been achieved. Clancy and Samimy (1997) have found that sub-pixel accuracy is required for good accuracy of the DGV method. **Fig. 11** shows an example of the ratio of dewarped dot card images for corresponding signal and reference cameras, to give an idea of the level of image overlay achieved.

The dewarped signal and reference images for each component are then divided, producing a ratio "image" containing values which are proportional to velocity. The ratio value for each pixel is passed through the inverted curve-fit of the appropriate cell calibration data found previously, resulting in a relative frequency value. The relative frequency values for pixel locations which have either signal or reference camera signal levels which are either saturated, or lie below a threshold of a gray scale level of 5 are marked and recorded. The frequency found from dividing the signal and reference voltages from the reference system and passing the resulting ratio through the reference curve-fit is then subtracted from both relative frequency arrays of the two components, to compensate for drift in laser frequency. The pixels marked as being saturated or having low gray level values are assigned a delta frequency value of zero, producing exactly zero velocity in the final velocity images. At this point, there exist two frequency "images" which are used in Equation 1 to produce two velocity images. Velocity images are actually floating point buffers which cannot be displayed normally, but when scaled from 0 to 255, can be viewed as grayscale or colorized images. The combination of system geometry and laser wavelength in Equation 1 yields a number that is a constant for each DGV component for a particular test setup. This number is called the component sensitivity because it quantifies the measured Doppler frequency shift per (m/sec) of velocity along the sensing direction. It has units of MHz/(m/sec), with typical values ranging from 2-3 MHz/(m/sec). The frequency images are simply divided by the corresponding sensitivity to produce velocity images as the final step in the data reduction process. These velocity images are then averaged, on an individual pixel basis, where zero velocity pixel values are omitted from the averaging. This is necessary for the pipe and jet velocity data, because of the drop off in signal near the edges of the flows, where there is a reduction in the amount of flow seeding.

SUMMARY OF PDV RESULTS

Early PDV data repeatability, as documented in the thesis by Ramanath (1997), was poor. The standard deviation of the slopes of plots of the measured PDV velocity versus the known velocity of a rotating wheel was on the order of 8-15 %, even though the linearity of each individual data set was quite good (on the order of ± 1-2 m/sec, out of 58 m/sec). Similar results were initially obtained by James (1997). However, the improved cell calibration procedures described above have significantly increased the accuracy of the present PDV system.

Typical examples of the present results for the rotating wheel will now be presented; these data are presented in much more detail in the thesis by James (1997). Data has been acquired in two different fashions: first, the 2-component PDV system was configured so that two simultaneous, but independent, measurements of the wheel velocity magnitude could be obtained, from two slightly different viewing directions. To do this, the system was set up so that both PDV channels had relatively good sensitivities in the wheel velocity direction. One channel (channel 2) was set up with a viewing direction which was at an angle of approximately 42 degrees from the laser propagation direction. The other channel (channel 1) viewed the wheel at an angle of approximately 75 degrees, by imaging the wheel off of a mirror which was mounted on the breadboard which held the channel 2 optical components (see **Fig. 5**). The wheel was inclined slightly (about 5 degrees) to the laser propagation direction. In this configuration, the resulting velocity data have been converted to wheel velocities by assuming that the direction of the wheel velocity was known. In the second configuration, the two PDV channels were set up with widely differing viewing angles (approximately 126 degrees from the laser propagation direction for channel 1, and approximately 42 degrees for channel 2), and the two PDV velocity measurements were used to resolve orthogonal x- and y-velocity components, from which the wheel velocity magnitude was computed as the square root of the sum of the squares of the components.

With the 2-component PDV system set up in the first configuration, a series of seven wheel velocity data sets were acquired, all using a single cell calibration data run (James, 1997). A typical example of the resulting data is shown in **Fig. 12**, where the measured PDV velocity magnitudes for channels 1 and 2 are shown plotted against the known wheel omega-r. Observed linearity is quite good. The standard deviations of the slopes of the linear curve fit equations from the correct slope of exactly 1.0 were calculated for several different curve fit options for each of the seven data sets. These errors ranged from a maximum of about ±15 % for a linear curve fit of the cell calibrations (on the same order of error as for the earlier data), to a low of ±1-2 % for a fourth-order curve fit. Specifically, from the individual slope results listed in Table 1, the deviations of the measured sensitivities were 1.4 % for channel 2 and 2.3 % for channel 1 using fourth- order curve fits to the calibration data. The accuracy to which the viewing angle could be measured was less for the channel which viewed the wheel off of the mirror (channel 1); this is believed to be the explanation for the larger error in sensitivity or slope for this channel. The actual standard deviations of the slope values are somewhat smaller, indicating that there is some bias error in these results; channel 2 slopes have a standard deviation of 1.1 %, while channel 1 slopes have a standard deviation of 1.5 %. Since the total range of wheel velocity for these measurements is about 58 m/sec, these observed 1-2 % errors correspond to velocity error magnitudes of approximately ±0.6-1.2 m/sec, which is quite good. Also, the standard deviations of the actual PDV velocity data points from the least squares linear curve fits have been computed, as listed in Table 1, and these errors are even smaller than the slope errors. For channel 2, the data for all seven runs display a standard deviation from a linear fit of 0.7 % (±0.4 m/sec), while channel 1 displays a standard deviation from a linear fit of 0.5 % (±0.3 m/sec). Again, this level of linearity is quite good. Since the errors in the slopes of the measured velocity versus omega-r were smallest using the fourth-order polynomial curve fits to the average ratio data, all subsequent PDV data has been reduced using this method. It has been observed that the reference cell is not able to consistently determine the zero velocity; thus, for the present results zero velocity has been fixed by a measurement of all voltage ratio values just prior to and after the actual data acquisition. Other researchers using scanned systems have had similar problems, which they have addressed by imaging a zero velocity region somewhere in each camera image (McKenzie, 1996, and Reinath, 1996; personal communication).

Table 1 Slope data for rotating wheel, set up with mirror and using known velocity direction

Run	Slope (Ch 1, Ch 2)	Deviation from linear fit (Ch 1, Ch 2, in m/sec)
1	1.0073, 1.0270	0.19, 0.26
2	0.9775, 0.9916	0.22, 0.35
3	0.9876, 1.0090	0.29, 0.40
4	0.9861, 0.9988	0.33, 0.50
5	0.9603,1.0046	0.37, 0.45
6	0.9747,1.0019	0.24, 0.46
7	0.9911,1.0142	0.35, 0.26

With the 2-component PDV system set up in the second configuration, a series of twelve wheel velocity data runs have been acquired, using five different cell calibrations (James, 1997). An example of this data is shown in **Fig. 13**, while the individual orthogonal velocity measurements are shown for this run in **Fig. 14**. The individual slopes and standard deviations of the data from a linear fit for each run have been given in Table 2. Here the standard deviation of the slopes of the linear curve fits to the data is 1 %, and the data points exhibit deviations from the linear curve fits with a standard deviation of 1.1 % (± 0.65 m/sec). Again, this is felt to be quite good accuracy. The accuracy of the channel 1 data, which is less sensitive to the wheel velocity, is not as good as that of channel 2. As a result, the accuracy of the computed x-velocity component, normal to the laser propagation direction, is not as good as the accuracy of the computed y-velocity component (**Fig. 14**). The correct sensitivities to the x- and y-velocity components, as shown in **Fig. 14**, were $\cos(5^{o})$ and $-\sin(5^{o})$.

Table 2 Slope data for rotating wheel; two-channel PDV set up

Run	Slope	Deviation from linear fit (m/sec)
1	0.9808	0.67
2	0.9981	0.50
3	0.9941	0.63
4	1.0073	1.34
5	1.0013	0.45
6	1.0080	0.99
7	1.0214	0.24
8	0.9996	0.35
9	0.9961	1.03
10	0.9928	0.42
11	0.9904	0.50
12	0.9989	0.69

During efforts to improve the accuracy of the point DGV system, typical RMS fluctuation levels of the voltage signals from the photodiodes have been monitored, along with the RMS fluctuation levels of the computed ratio of signal-to-reference voltages. For the reference system, RMS voltage fluctuations typically are on the order of 0.5 % of the mean voltage for each photodiode, but the RMS fluctuation in the ratio is approximately 0.2 % of the mean ratio value. Similar percentage fluctuations in the ratio value have been observed during experiments using the rotating wheel. Recently, a simple math model of this phenomenon has been proposed by Ramanath, where the individual signals from the photodiodes are modeled as sine functions, each of which can have offset and/or phase errors. The ratio of these two model signals can show increased, "spiky" fluctuation levels, as is sometimes observed in the data when the raw voltage levels are small. Offset errors may occur due to inaccuracies or changes in the detector dark or background voltages; such errors become more significant as the signal level decreases.

An analysis of the major error sources for the present PDV results has been performed, as briefly summarized below.

1. The accuracy to which the rotating wheel speed has been set has been checked by using a strobe and measuring the time between voltage spikes in the output of one of our PDV signal photodiodes, using an oscilloscope. The reading error for these time measurements was estimated to be no greater than ± 0.5 %, which is about the same as the observed accuracy to which the individual PDV data points fit to a least-squares straight line. To do any better than this at checking the linearity of response of the instrument, the individual wheel speed settings would need to be measured with greater accuracy, for each data point.

2. The level of zero velocity drift of the 2-component PDV system has been measured for a period of 30 minutes, as shown in the **Fig. 15**. The observed drift in zero velocity is on the order of ± 1.5 m/sec; this is thought to be primarily due to drift in cell stem temperatures, as shown in **Fig. 16**, where the difference between the stem temperature for the PDV signal channel, and the reference cell stem temperature, is shown for each channel, for the same time period as the zero velocity data run (**Fig. 15**). The similarity of the shapes of these two graphs indicates that this error is due primarily to the combination of the accuracy of the cell stem temperature controllers and the accuracy of the calibration curves. It is also felt that this drift in cell stem temperature difference is a significant contributor to the observed error in sensitivity of the two PDV channels. However, no correlation has been found between the slope data given in Tables 1 and 2, and the stem temperature difference values for each data run. It is noted that the present zero velocity drift (± 1.5 m/sec) is reduced relative to the earlier results presented by Ramanath (1997), of ± 4 m/sec; this is due to the improved accuracy of the present cell calibrations.

3. Using four of the five calibration curves which have been used to reduce the second series of wheel velocity data, the repeatability of the calibration curves from day-to-day has been investigated (James, 1997), by forcing pairs of corresponding calibration curves to overlay exactly at the middle of the ratio range which was actually used to reduce the wheel velocity data, and computing the difference in computed velocities which would result at the top and bottom of these ratio ranges if the two different cell calibrations were used to reduce the same wheel velocity data set. (See **Fig. 17** for an example.) The resulting errors were found to be between 2.3 and 0.3 m/sec, with and average error of 0.7 m/sec. (± 1.2 %). These errors due to using different cell calibrations are on the same order as the observed error in slopes of the wheel velocity data results. As a result, it is believed that while the current cell calibration procedure has led to a significant improvement in results, the primary error source in the current PDV system is still the accuracy of the cell calibrations. To improve this accuracy further, work is underway to implement the curve-fitting procedure described by McKenzie (1995), which uses the theoretical iodine cell absorption curve calculated by the Forkey theoretical cell absorption model to curve fit the actual cell calibration data. It is felt that this procedure will remove the judgment which is required in the current polynomial curve fit technique, where the user must decide which portion of the cell calibration data to include in the curve fit process. Also, from **Fig. 17** it is noted that the useful range of the developed PDV system is on the order of 100-200 m/sec; this range can be increased by the addition of a neutral buffer gas to the iodine vapor (Elliott, et al., 1994). A reduction in this useful range, in hopes of increasing the resolution of the Doppler velocimeter, may be possible through use of a Cesium Faraday filter (Bloom, et al., 1993).

An example of two-component PDV data obtained from a traverse across the exit of the fully-developed pipe flow apparatus, at a nominal Reynolds number of 76,000, is shown in **Figs. 18 and 19.** These results are the averages of four successive continuous traverses across the pipe exit, at a nominal Reynolds number of 76,000. The traverse rate was 0.1 inch/sec, and the PDV sampling rate was 100 samples/sec. To compute average and RMS values, binning of the raw data has been performed. Ten point, binned, average and RMS values have been computed for each traverse, and these results have been averaged for the four traverses. In the time required to acquire ten data values, the traverse moved 0.01", while the PDV probe volume is estimated to be approximately 2 mm in diameter. These 10 point averages and RMS values have been displayed in **Figs. 18** and **19**. The axial mean velocities agree reasonably well with results from a pitot-static probe survey, but radial mean velocities currently display an offset error on the order of 2-4 m/sec (**Fig. 18**). Turbulence intensities (**Fig. 19**) agree well with the hot wire data of Laufer (1954). Note that measured axial RMS velocities are larger than measured circumferential velocities, also consistent with Laufer's data. There are significant difficulties near the pipe walls, both due to reduced signal-to-noise levels due to less smoke, as well as to reflections of the scattered light off of the pipe walls. However, at present the greatest difficulty appears to be obtaining accurate, reliable zero velocity ratio values.

DGV RESULTS

Introduction

The results presented in this section are from a two-component DGV setup represented schematically for the wheel velocity data runs in **Fig. 20**. Results have been obtained for a rotating wheel, and fully-developed, turbulent pipe flow. The beam exits the laser and enters the X-Y scanner head, which, for recording wheel velocity data, is stationary and simply acts as a turning mirror. This X-Y scanner has been used to generate a laser light sheet that has been used to illuminate cross sectional cuts of the pipe and jet flows.

For the wheel velocity data, the beam is steered through a 9mm focal length biconvex lens, creating a cone of laser light that is projected onto the surface of the wheel. Since the lens is small (9mm OD) and coherent light is passing through it, imperfections on the surface of the lens create a series of circular interference fringes which are visible on the surface of the wheel. Two layers of opaque plastic film placed in the expanded beam serve as optical diffusers which effectively remove any visible intensity variations (McKenzie, 1997). The DGV sensing components have been placed at shallow angles with respect to the incident laser beam to maximize their sensitivity to the direction of motion of the wheel. For the angles shown, components 1 and 2 have sensitivities of 2.19 and 3.07 MHz/(m/sec), respectively. Further, component 2 is aligned so that it measures 82 % of the wheel velocity, compared to 65 % for component 1. This implies that less accurate and noisier readings should be expected for component 1, which has been confirmed by the data to be presented below.

Wheel Velocity DGV Results

Four sets of rotating wheel data have been acquired; two sets at a wheel setting of maximum speed clockwise, and two sets at maximum speed counter-clockwise. Each set was taken on the same day and reduced using the same cell calibrations (**Fig. 8**), which were acquired just before the velocity data. Typical results from DGV component 2 will be shown in detail since that component has the greatest sensitivity to wheel velocity, and thus represents the best available data. **Fig. 21** shows horizontal and vertical cuts through the average of 30 velocity images for the second component. For the motor speed setting used, and the diameter of the wheel, the calculated full velocity range (top to bottom) is 58.7 m/sec. An offset on the order of 5 m/sec in the DGV measurements has been subtracted from both cuts. The cause of this zero velocity offset is presently unknown; similar zero offsets were observed in the point PDV results of Kuhlman, et al. (1997). An analysis of all four wheel data sets is summarized in Table 3.

Table 3. Analysis of non-zero DGV wheel velocity data sets.

Data Run	Y Velocity Range (m/s)	Percent Error	RMS (m/s) X cut, Y cut
1	60.1	2.4 %	1.2, 1.3
2	60.2	2.6 %	1.2, 1.3
3	57.8	1.5 %	0.9, 1.2
4	58.2	0.9 %	0.9, 1.3

The Y velocity range has been found by placing a least-squares linear fit through a vertical cut taken down the center of the velocity image and subtracting the two endpoint values of the fit. Percent error has been calculated with respect to the correct range of 58.7 m/s for all runs. The last column lists RMS deviations for an X (horizontal) cut through the center and the RMS difference from a linear fit through a Y (vertical) cut. All four of these runs are the processed average of 30 images. Values for a randomly selected single image are 59.0 m/sec vertical range which corresponds to 0.05 % error, and RMS values of 1.5 and 2.0 m/sec for X and Y cuts, respectively. For the first component, typical values are 48.2 m/sec, 18 % error for the vertical cut, and RMS values of 3.9 m/sec and 3.7 m/sec. The increased RMS values can be mostly attributed to the poor sensitivity value of the first component due to geometry constraints. However, the positioning of the component does not explain the 18 % error in the vertical velocity range; this 10.5 m/sec error is the largest which has been observed in these initial studies. Inconsistencies in the cell calibrations result in bias errors, which are partly responsible for the errors in the velocity range. Analysis of the curve fits from two sets of calibrations performed on different days, produces a maximum error of ~2.4 m/sec or 4 %, based on the maximum ratio range recorded by the data images.

Pipe Velocity DGV Results

Eight sets of pipe flow velocity measurements were taken, each set consisting of 30 individual images. Two sets each were taken at 0, 2/3, 4/3, and 2 diameters from the pipe exit. For brevity, results will be shown only for one set at the exit station. **Fig. 22** shows horizontal and vertical cuts through an average of 30 velocity images taken at the pipe exit. In a region near the pipe exit, a small piece of poster paper was placed visible to both components and illuminated with a small amount of laser light via a fiber optic cable. This produced a zero velocity reference tab which has been averaged and subtracted from each individual velocity image (McKenzie, 1997). For the data shown, a 4.8 m/s offset has been subtracted. The peak velocity on the centerline of the pipe as measured by a pitot probe was 35 m/s, in reasonable agreement with the DGV results. A noticeable error in the horizontal cut near the right hand side of the image is due to light reflected off of the lip of the pipe, showing the type of error that can be caused by this effect. Velocity variation near the pipe walls is believed to be more accurate for the DGV data (**Fig. 22**) than for the PDV data (**Fig. 18**). This is due to the larger probe volume for the PDV system (James, 1997), which causes spatial averaging of the data.

CONCLUSIONS

The development of a two-component Point Doppler Velocimeter (PDV) has been described. Accuracy of the present PDV system, based on the rotating wheel velocity results, has been documented to be on the order of ± 0.6 m/sec over a velocity range of 57 m/sec (ie, approximately ± 1 % of full scale). Linearity of the present PDV system, again based on the wheel data, has been documented to be on the order of ± 0.3 m/sec, which is on the order of the accuracy of the individual wheel velocity settings; this linearity is on the order of 0.5 % of the measured velocity range. Both of these observed accuracy measurements are considerably better than those documented to date by other researchers. Two-component PDV velocity data have been presented for a fully-developed turbulent pipe flow, at a Reynolds number of approximately 76,000. Turbulence intensity values agree well with earlier hot wire data, and mean axial velocity data agree reasonably well with pitot tube results. However, circumferential mean velocity results show a consistent offset error which is on the order of ten percent of the mean axial velocity; the reasons for this error are at present uncertain, but are believed to be due to inaccuracy in the determination of zero velocity or inaccuracies in the cell calibrations.

The development of a two-component Doppler Global Velocimeter (DGV), along with the corresponding image acquisition and data reduction software, has also been described. This DGV system has been patterned after similar systems developed at NASA Langley Research Center. Results from this system have been presented for the velocity distribution on a rotating wheel and fully-developed turbulent pipe flow. For the configuration used, the DGV images of the rotating wheel display the expected horizontal bands of constant horizontal wheel velocity. The RMS deviation of the DGV data from a linear wheel velocity variation in the Y image direction was found to be ±1.1 m/sec, for a single DGV component. This corresponds to about ±2 % of the 58 m/sec velocity range for the present experiments. RMS deviations of the constant velocity values along X cuts through data images were also found to be ±0.9 m/sec. The discretization visible in the velocity cuts suggests that the dominant error source is the 8 bit limitation of the camera/frame grabber combination. If this is the case, then the percent error could be reduced somewhat by maximizing the component sensitivity and/or increasing the measured velocity range. Observed errors in the total measured variation in horizontal velocity across the vertical (Y) extent of the wheel ranged from 1-2 m/sec. Much of this sensitivity error was believed to be due to inaccuracies in the cell calibrations. A zero velocity offset has been observed for all of the present results; the cause of this offset is presently unknown. A similar zero offset was observed in the PDV results of Kuhlman, et al. (1997). A zero velocity reference tab, illuminated by the unshifted laser light, has been used to correct for this error in the DGV results.

PERSONNEL

In addition to the PI, two MS students and one PhD student have worked on the project. Both MS students have completed their degrees (Ramanath, 1997; James, 1997), while the PhD student is expected to complete his degree by July, 1998.

TRANSITIONS

The new iodine cell calibration procedure developed as a part of this work has been evaluated and adopted by the NASA Langley DGV research team for use with their Argon ion laser DGV system, and has demonstrated improved calibration accuracy.

ACKNOWLEDGMENT/DISCLAIMER

The present work has been supported under AFOSR/DEPSCoR Grant F49620-94-1-0434, Dr. James M. McMichael and Dr. Mark Glauser, technical monitors, as well as NASA Langley Research Center Grants NAG-1-1892 and NAGW-4464. The author is grateful for the technical assistance of Jim Meyers, Joe Lee, Rich Schwartz, Angelo Cavone, and Gary Fleming at NASA Langley Research Center, Bob McKenzie and Mike Reinath at NASA Ames Research Center, and Tom Beutner of the Wright Laboratory. The views and conclusions contained herein are those of the author and should not be interpreted as necessarily representing the official policies or endorsements, either expressed or implied, of the Air Force Office of Scientific Research or the U. S. Government.

REFERENCES

Adrian, R. J. and Yao, C. S., "Development of Pulsed Laser Velocimetry for Measurement of Turbulent Flow," Proc. of the Eighth Biennial Symposium on Turbulence, Univ. of Missouri, Rolla, 1983, pp. 170-186.

Beutner, T. J. and Baust, H. D., "Recent Developments in Doppler Global Velocimetry," paper no. 8 of AGARD Fluid Dynamics Panel 81st Meeting/Symposium on Advanced Aerodynamic Measurement Technology, Sept. 22-25, 1997, Seattle, WA.

Bloom, S. H., Searcy, P. A., Choi, K., Kremer, R., and Korevaar, E., "Helicopter Plume Detection by Using an Ultranarrow-Band Noncoherent Laser Doppler Velocimeter," Optics Letters, Vol. 18, No. 3, Feb. 1993, pp. 244-46.

Clancy, P. S. and Samimy, M., "Multiple-Component Velocimetry in High Speed Flows Using Planar Doppler Velocimetry," paper AIAA-97-0497, AIAA 35th Aerospace Sciences Meeting, Jan. 6-10, 1997, Reno, NV.

Dahm, W. J. A., "Scalar Imaging Velocimetry Studies of Turbulent Flow Structure and Dynamics," AFOSR/ONR Grantee and Contractors Meeting on Turbulence Research, Chicago, IL, June 10-12, 1992; pp. 73-76 of Workshop Proceedings.

Elliott, G. S., Mosedale, A., Gruber, M. R., Nejad, A. S., and Carter, C. D., "The Study of a Transverse Jet in a Supersonic Cross-Flow Using Molecular Filtered Based Diagnostics," paper AIAA-97-2999, presented at AIAA/ASME/SAE/ASEE Joint Propulsion Conference, July 6-9, 1997, Seattle, WA.

Elliott, G.S., Samimy, M., and Arnette, S. A., "Details of a Molecular Filter-Based Velocimetry Technique," paper AIAA - 94-0490, AIAA 32nd Aerospace Sciences Meeting, Jan. 10-13, 1994, Reno, NV.

Forkey, J. N., Finklestein, N.D., Lempert, W. R., and Miles, R. B., "Control of Experimental Uncertainties in Filtered Rayleigh Scattering Measurements," paper AIAA-95-0298, presented at AIAA 33rd Aerospace Sciences Meeting, Jan. 9-12, 1995, Reno, NV; also AIAA Journal, vol. 34, No.3, Mar. 1996, pp. 442-448.

Hoffenberg, R. and Sullivan, J. P., "Filtered Particle Scattering: Laser Velocimetry Using an Iodine Filter," ASME Fluids Engineering Division Summer Meeting, Washington, DC, June 2024, 1993.

Irani, E., "Application and Evaluation of the Doppler Global Velocimetry Method on an Axi-Symmetric Jet," Ph.D. Dissertation, Wichita State University, May, 1995.

Irani, E. and Miller, L. S., "Evaluation of a Basic Doppler Global Velocimetry System," SAE paper 951427, Aerospace Atlantic Conference, May 23-25, 1995, Dayton, OH.

James, K., "Determination of the Accuracy of a Two-Component Point Doppler Velocimetry System," MS Thesis, West Virginia University, MAE Department, 1997.

Komine, H., U.S. Patent No. 4, 919, 536 Apr. 24, 1990.

Kuhlman, J. M., "Turbulence Measurements in Annular Jets Using Laser Velocimetry", ASME Symp. Laser Anemometry: Advances and Applications, Lake Tahoe, NM, June 19-23, 1994, published in ASME FED Vol. 191, pp. 77-82.

Kuhlman, J. M., Naylor, S., James, K., and Ramanath, S., "Accuracy Study of a 2 Component Point Doppler Velocimeter (PDV)," paper AIAA-97-1916, presented at AIAA 28th Fluid Dynamics Conference, Snowmass, CO, June 29-July 2, 1997.

Laufer, J., "The Structure of Turbulence in Fully Developed Pipe Flow," NACA TR 1174, 1954.

McKenzie, R. L., "Measurement Capabilities of Planar Doppler Velocimetry Using Pulsed Lasers," paper AIAA-95-0297, AIAA 33rd Aerospace Sciences Meeting, Jan. 9-12, 1995, Reno, NV; also Applied Optics, Vol. 35, No. 6, Feb. 1996, pp. 948-964.

McKenzie, R. L., "Planar Doppler Velocimetry Performance in Low-Speed Flows," paper AIAA-97-0498, ALAA 35th Aerospace Sciences Meeting, Jan. 6-10, 1997, Reno, NV.

Meyers, J. F. and Komine, H., "Doppler Global Velocimetry: A New Way to Look at Velocity," 4th International Conference on Laser Anemometry, Advances and Applications, Aug. 5-9, 1991, Cleveland, OH, pp. 289-296 of Conference Proceedings.

Meyers, J. F., Lee, J. W., and Cavone, A. A., "Signal Processing Schemes for Doppler Global Velocimetry," 14th International Congress on Instrumentation in Aerospace Simulation Facilities, Rockville, MD, Oct. 27-31, 1991.

Meyers, J. F., "Doppler Global Velocimetry, The Next Generation?," paper AIAA-92-3897, presented at AIAA 17th Ground Testing Conference, July 6-8, 1992, Nashville TN.

Meyers, J. F., "Evolution of Doppler Global Velocimetry Data Processing," 8th Int'l. Symp. On Applications of Laser Techniques to Fluid Mechanics, July 8-11, 1996, Lisbon, Portugal.

Miles, R. B., "RELIEF Measurements of Turbulence," AFOSR/ONR Grantee and Contractors Meeting on Turbulence Research, Chicago, IL, June 10-12, 1992; pp. 62-64 of Workshop Proceedings.

Miles, R. B., Lempert, W.R., and Forkey, J., "Instantaneous Velocity Fields and Background Suppression by Filtered Rayleigh Scattering," paper AIAA-91-0357, AIAA 29th Aerospace Sciences Meeting, Jan. 7- 10, 1991, Reno, NV.

Morrison, G. L., Gaharan, C.A., and DeOtte, R. E., Jr., "Doppler Global Velocimetry: Problems and Pitfalls," Symposium on Laser Anemometry: Advances and Applications, June 1923, 1994, Lake Tahoe, NV, published in ASME FED Vol. 191, pp. 1-8.

Naylor, S. and Kuhlman, J., "Accuracy Studies of a Two-Component Doppler Global Velocimeter (DGV)," paper AIAA-98-0508, AIAA 36th Aerospace Sciences Meeting, Jan. 12-15, 1998, Reno, NV.

Ramanath, S., "Development of a Point Doppler Global Velocimeter (DGV)," MS Thesis, West Virginia University, MAE Department, 1997.

Reinath, M. S., "Doppler Global Velocimeter Development for the Large Wind Tunnels at Ames Research Center," NASA TM-112210, Sept. 1997.

Roehle, I. and Schodl, R., "Evaluation of the Accuracy of the Doppler Global Technique," paper C485/046, Seminar on Optical Methods and Data Processing in Heat and Fluid Flow, Apr. 14-15, 1994, City Univ., London, UK.

Smith, M. W. and Northam, G. B., "Application of Absorption Filter-Planar Doppler Velocimetry to Sonic and Supersonic Jets," paper AIAA-95-0299, AIAA 33rd Aerospace Sciences Meeting, Jan. 9-12, 1995, Reno, NV; also AIAA J., Vol. 34, No. 3, Mar. 1996, pp. 434-441.

Wolberg, G., Digital Image Warping, IEEE Computer Society Press, Los Alamitos, CA, 1990.

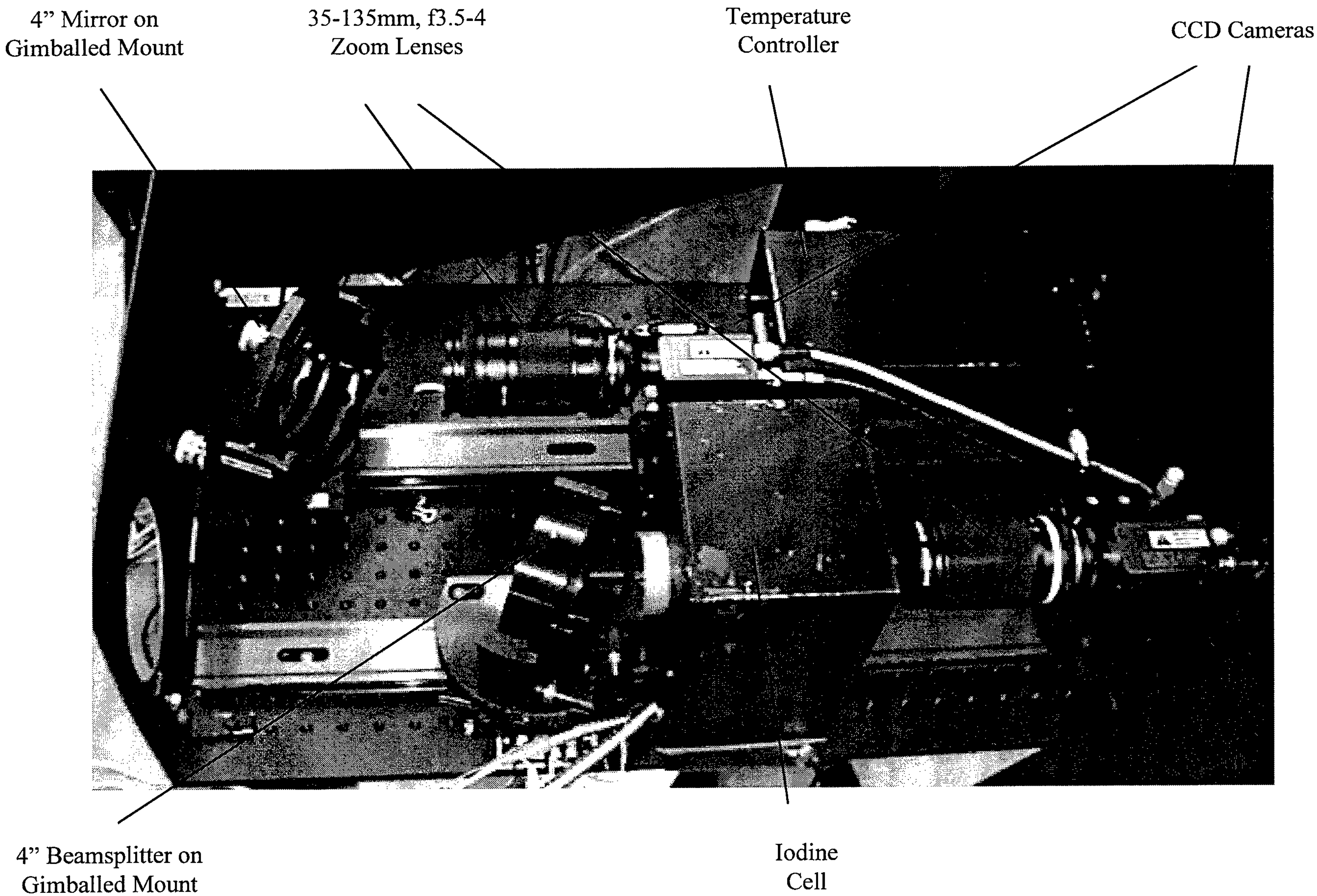

Fig. 1. Top view of a DGV velocity measuring component.

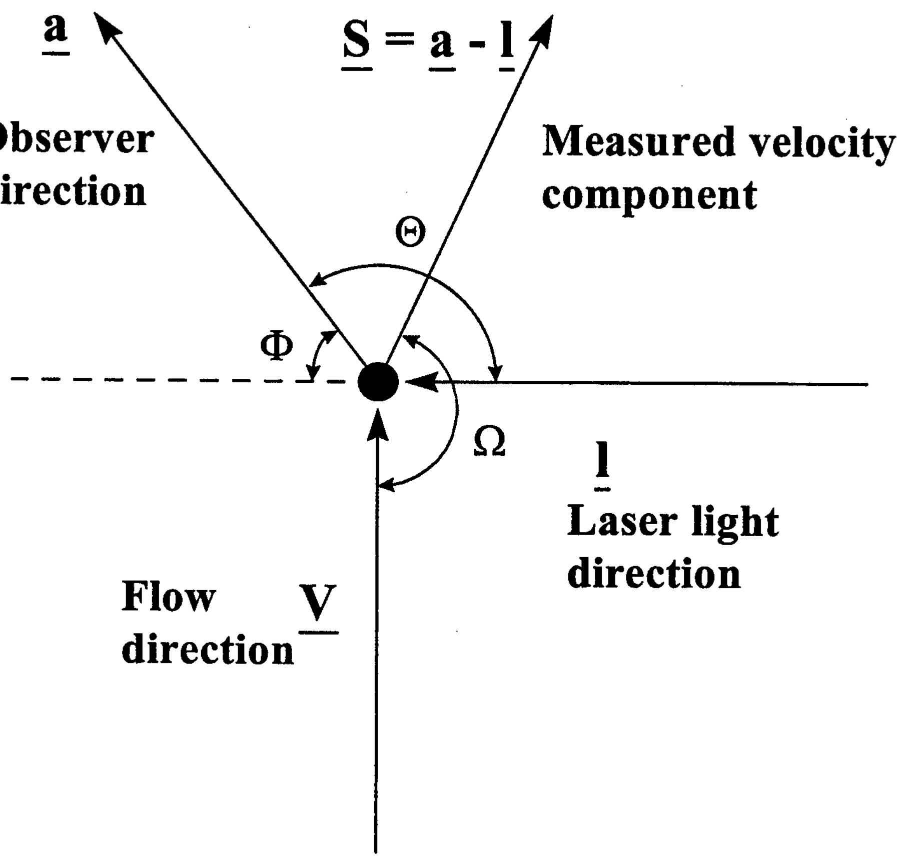

Fig. 2 Vector geometry for PDV and DGV systems

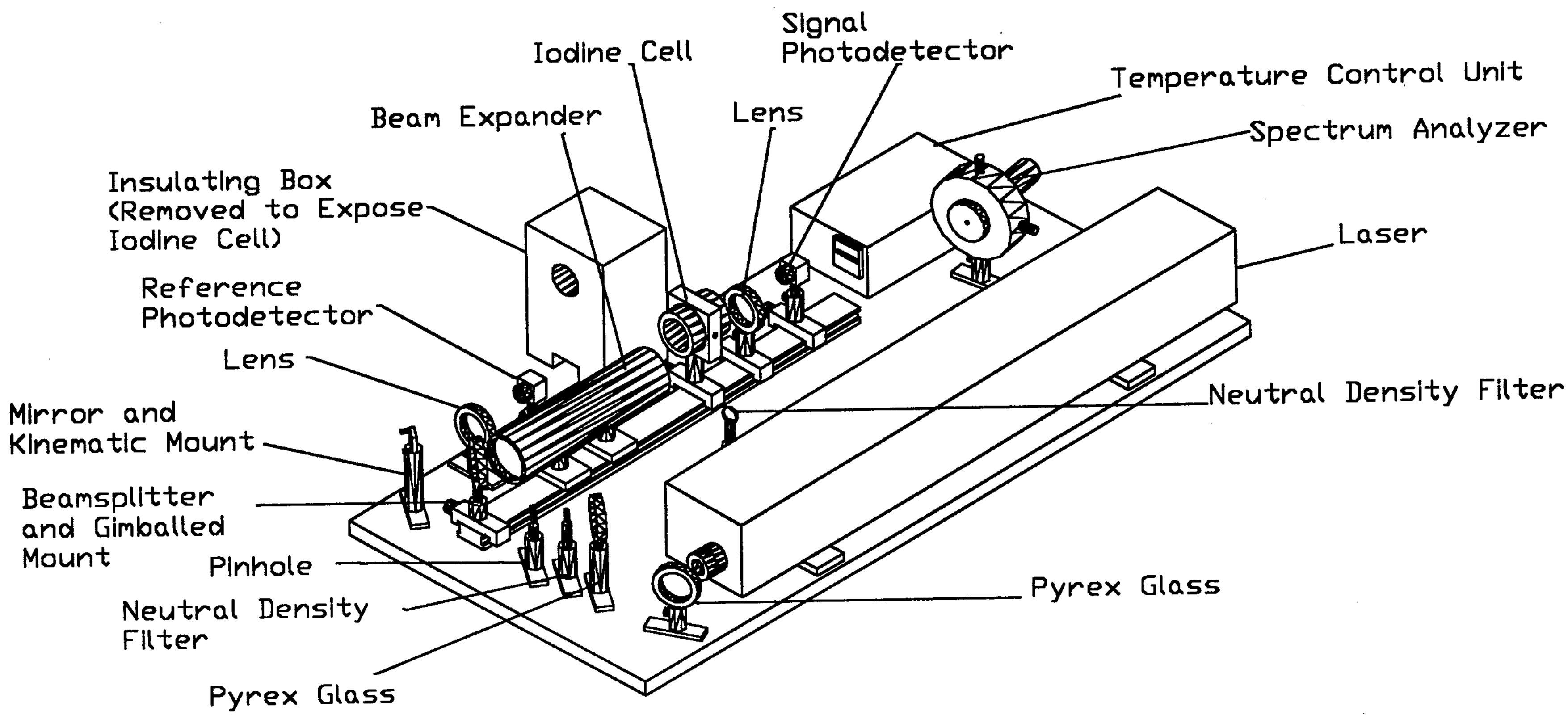

Fig. 3 Apparatus for reference iodine cell system, laser, and spectrum analyzer

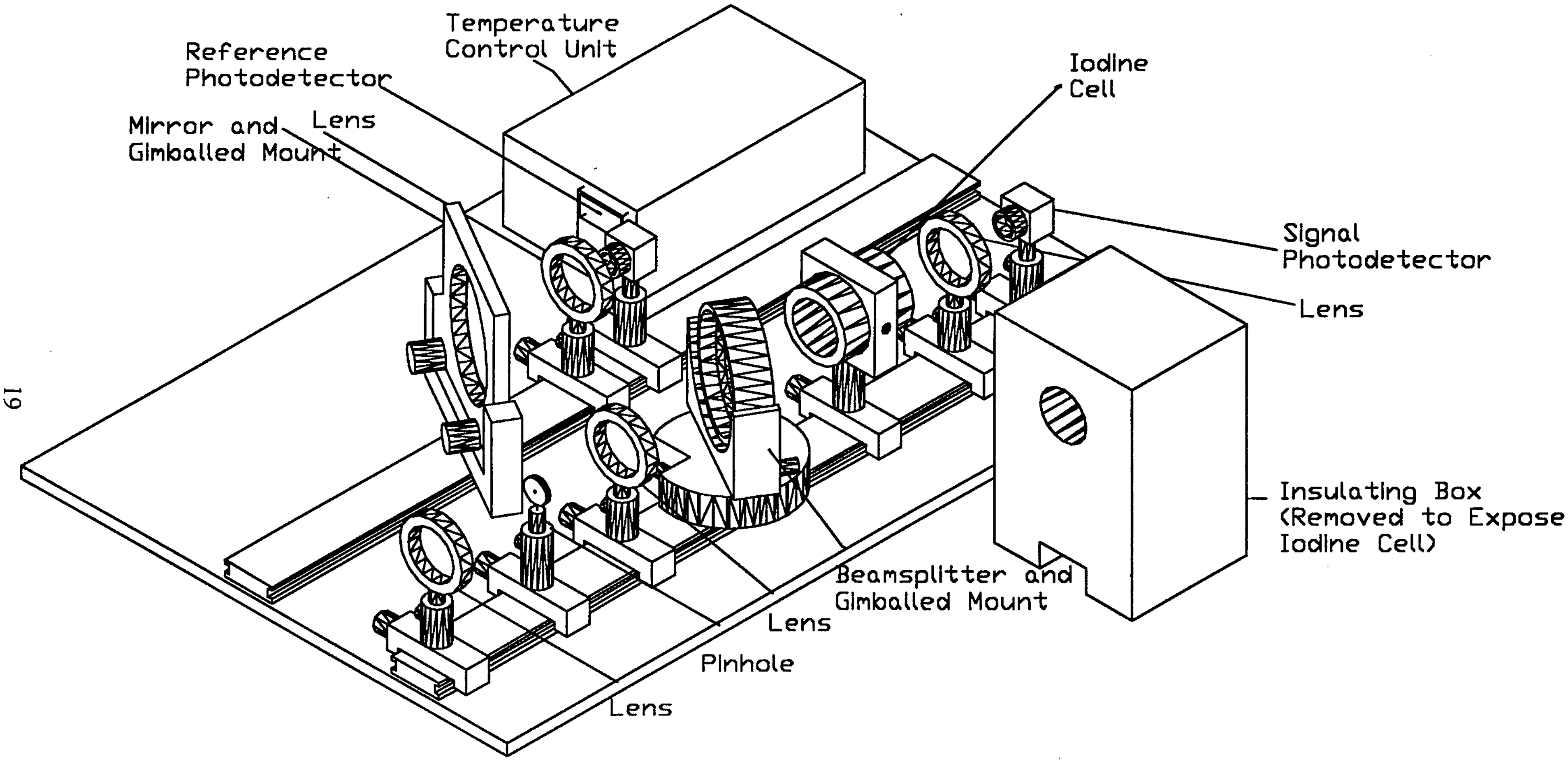

Fig.4 Apparatus for one PDV channel

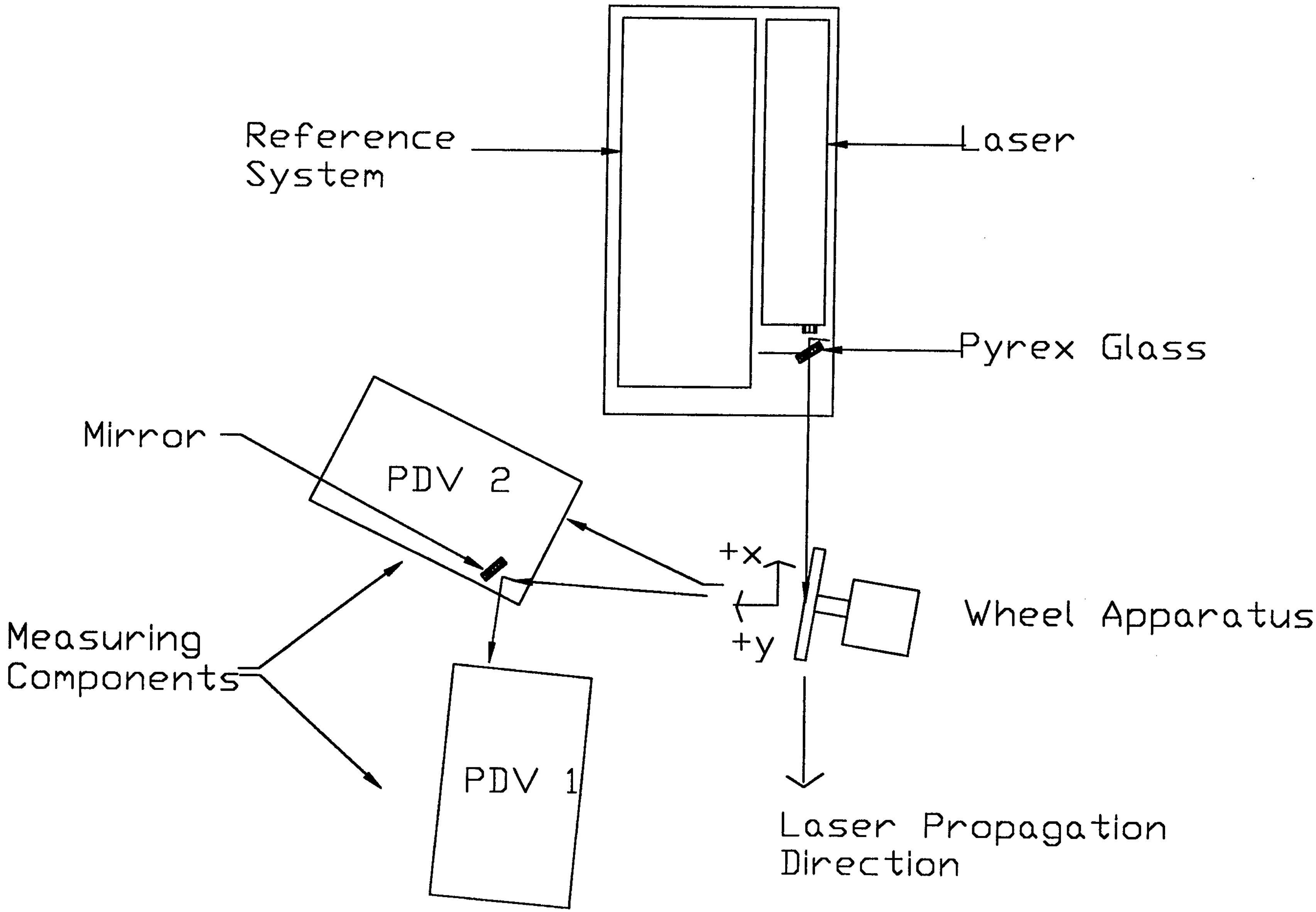

Fig. 5 Schematic of two-component PDV apparatus set-up, viewed from above, for wheel velocity measurements

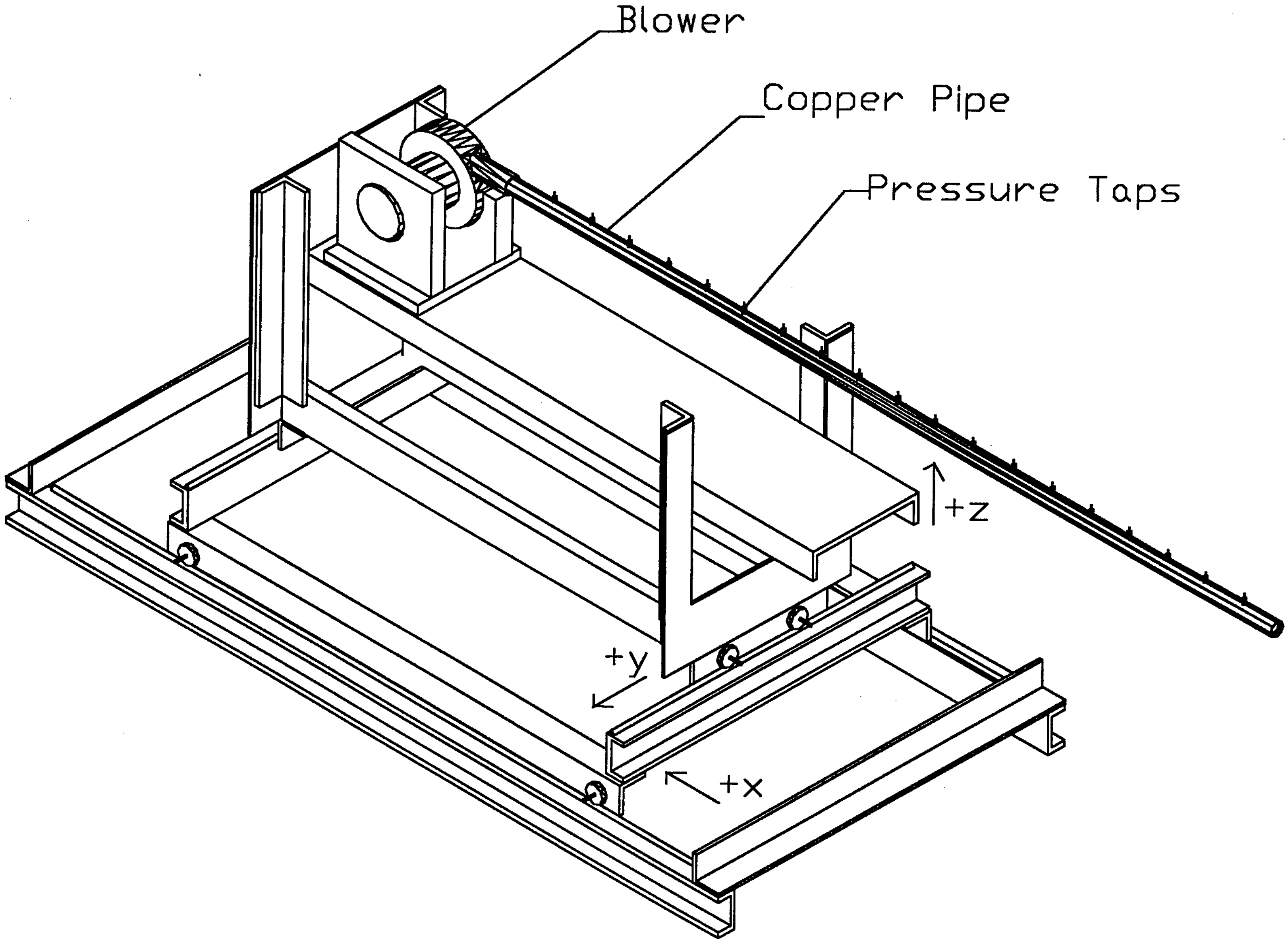

Fig. 6 Three-axis traverse system, shown with fully-developed turbulent pipe flow apparatus

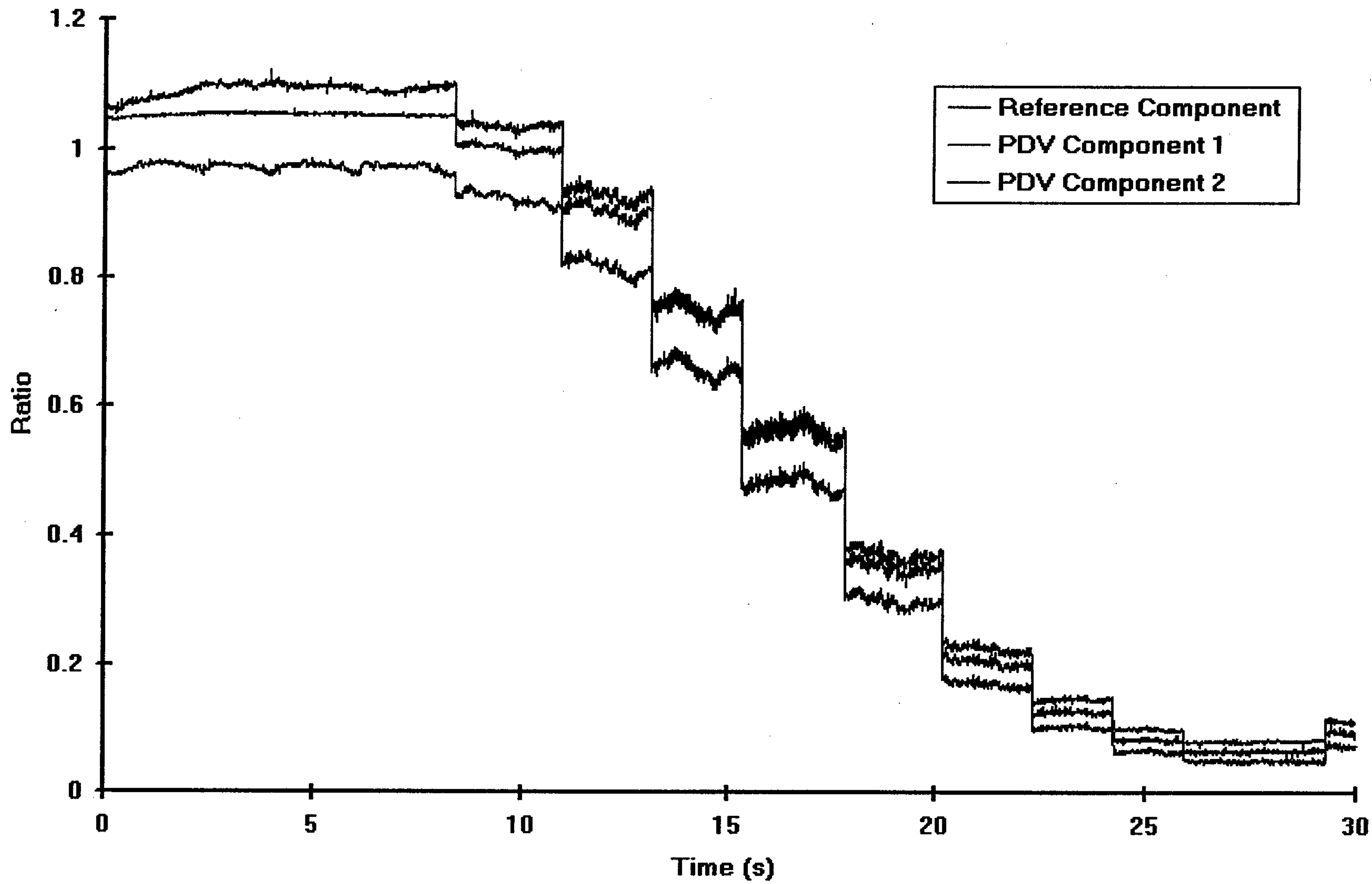

Fig. 7 Continuous scan mode hop calibration data for CW Argon Ion laser

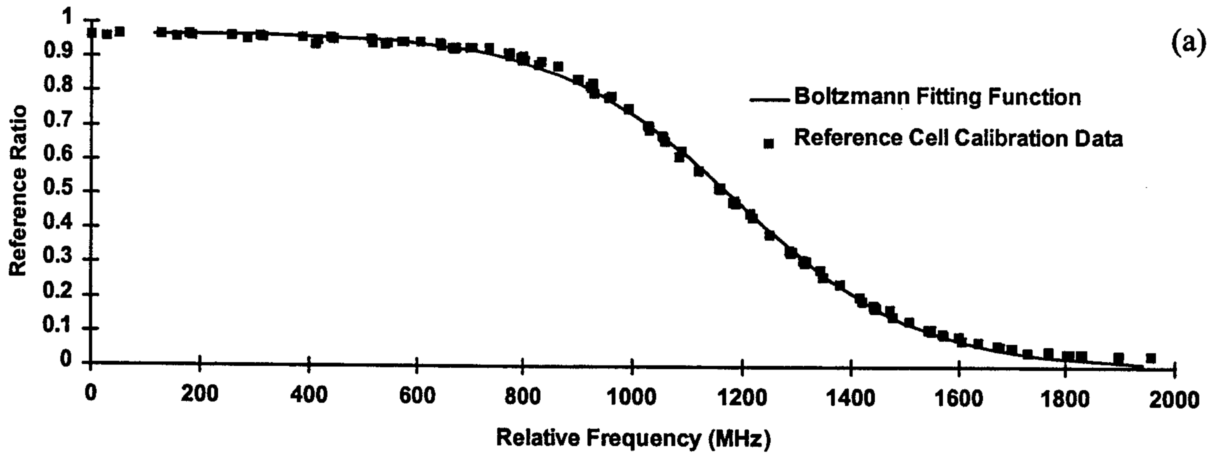

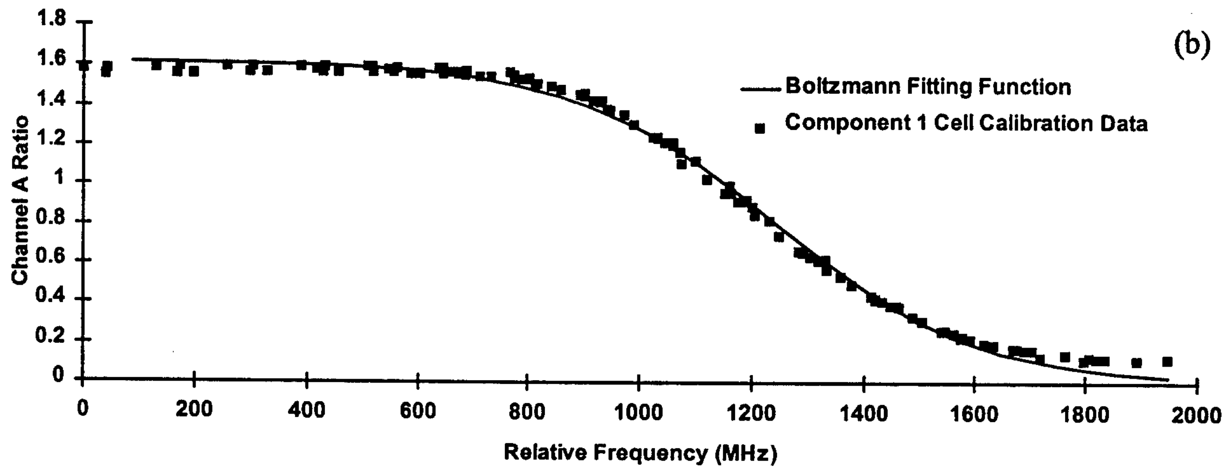

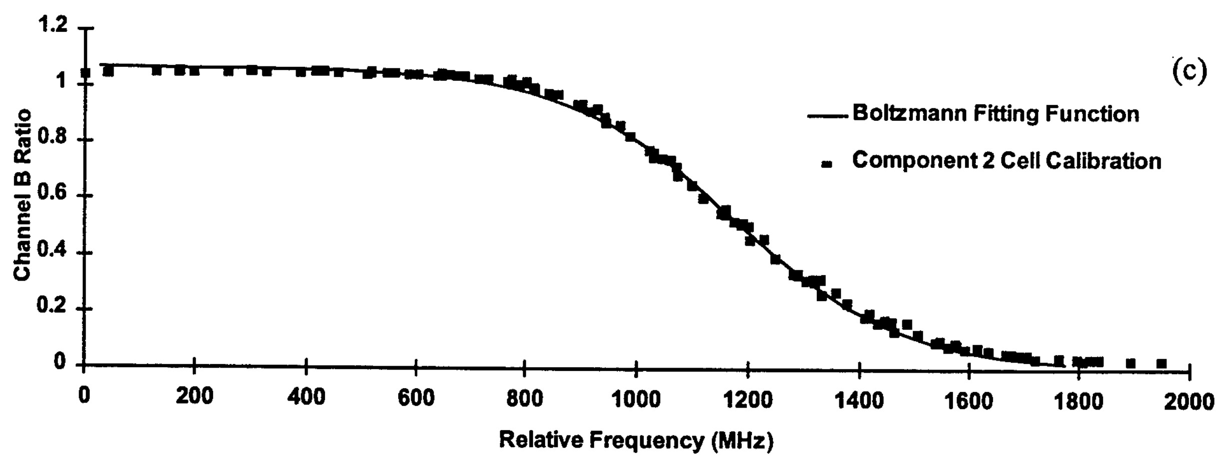

Fig. 8 Calibration data and curve fits for the Reference (a), Component 1 (b), and Component 2 (c) channels.

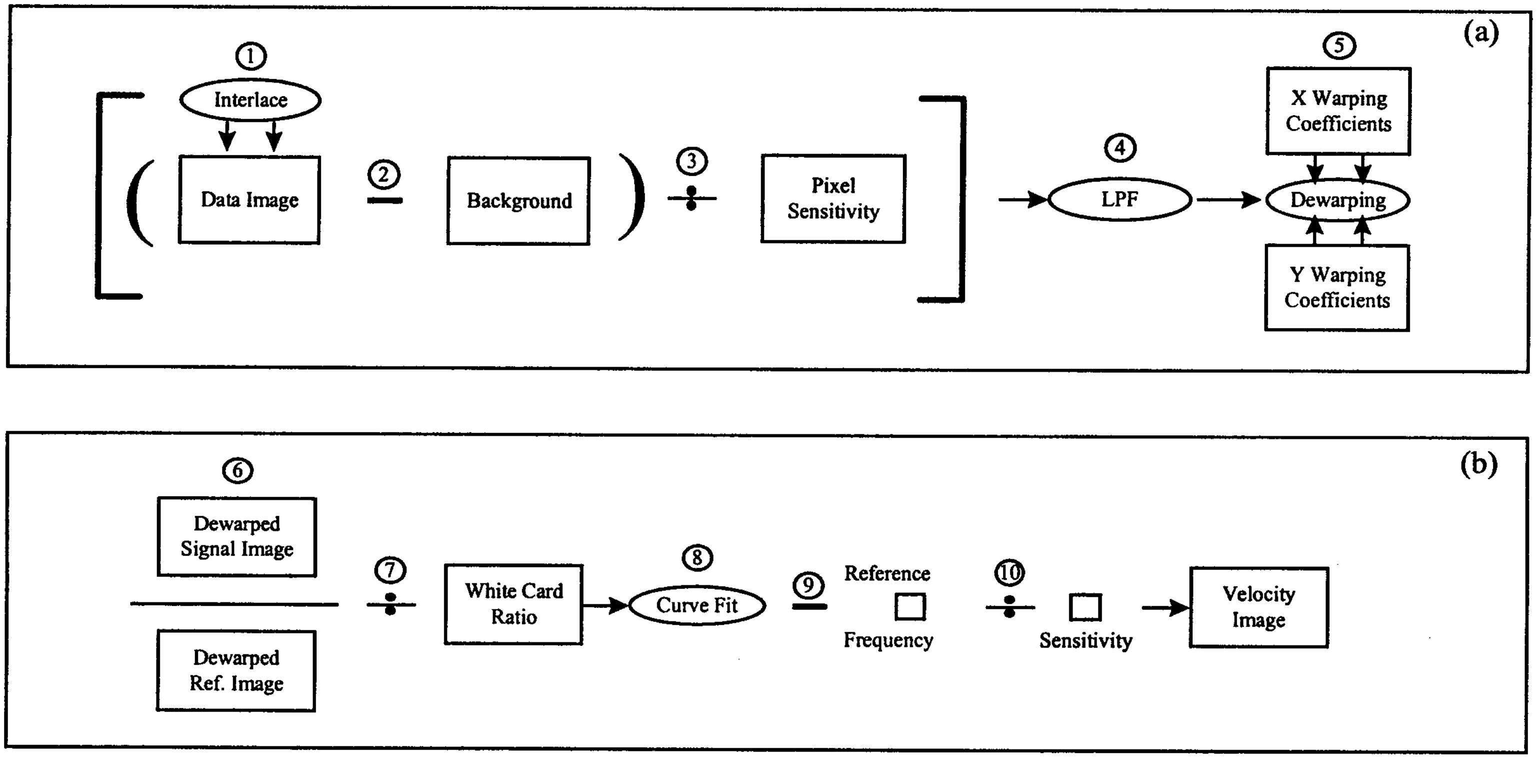

Fig. 9 Block diagram of image processing steps. Steps 1-5 (a) are performed on each image, while in steps 6-10 (b), signal and reference images are combined to generate a velocity image.

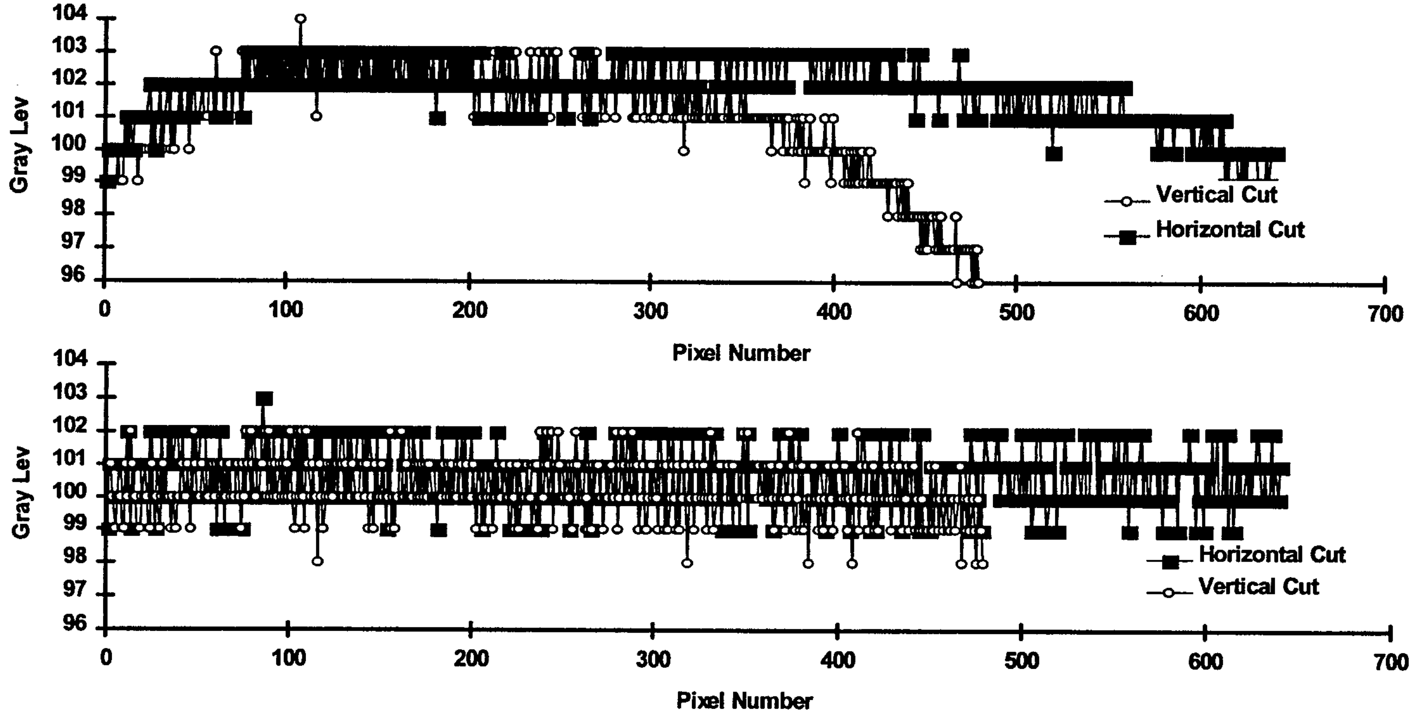

Fig. 10 Cuts through a flat field image before (a) and after (b) the pixel flattening correction was applied. Vertical and horizontal RMS variations are ±1.6 and ±0.9 before flattening, and both have a value of 0.8 after.

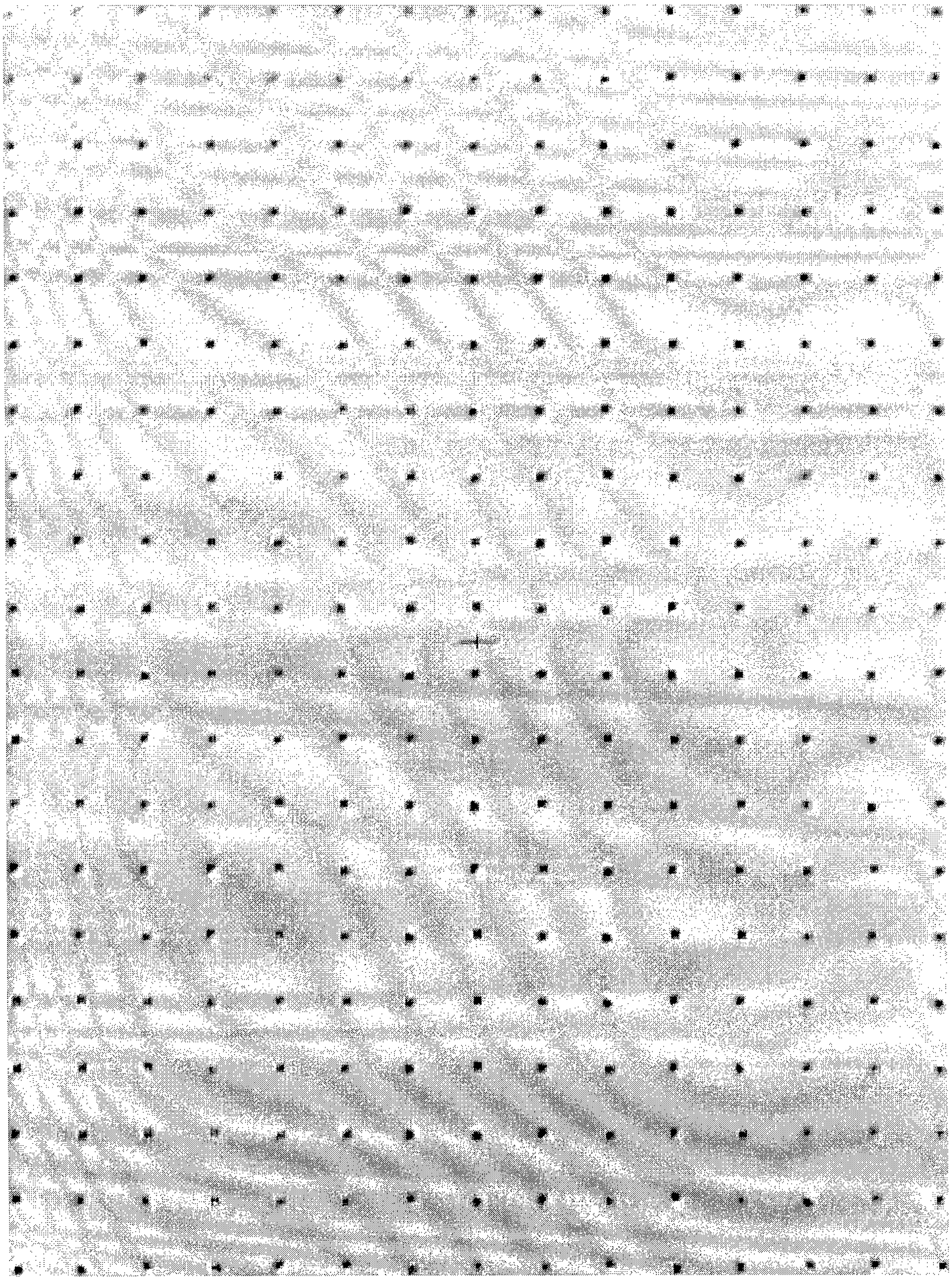

Fig. 11 Ratio of signal and reference camera dewarped dot card images for the 1st component showing pixel registration

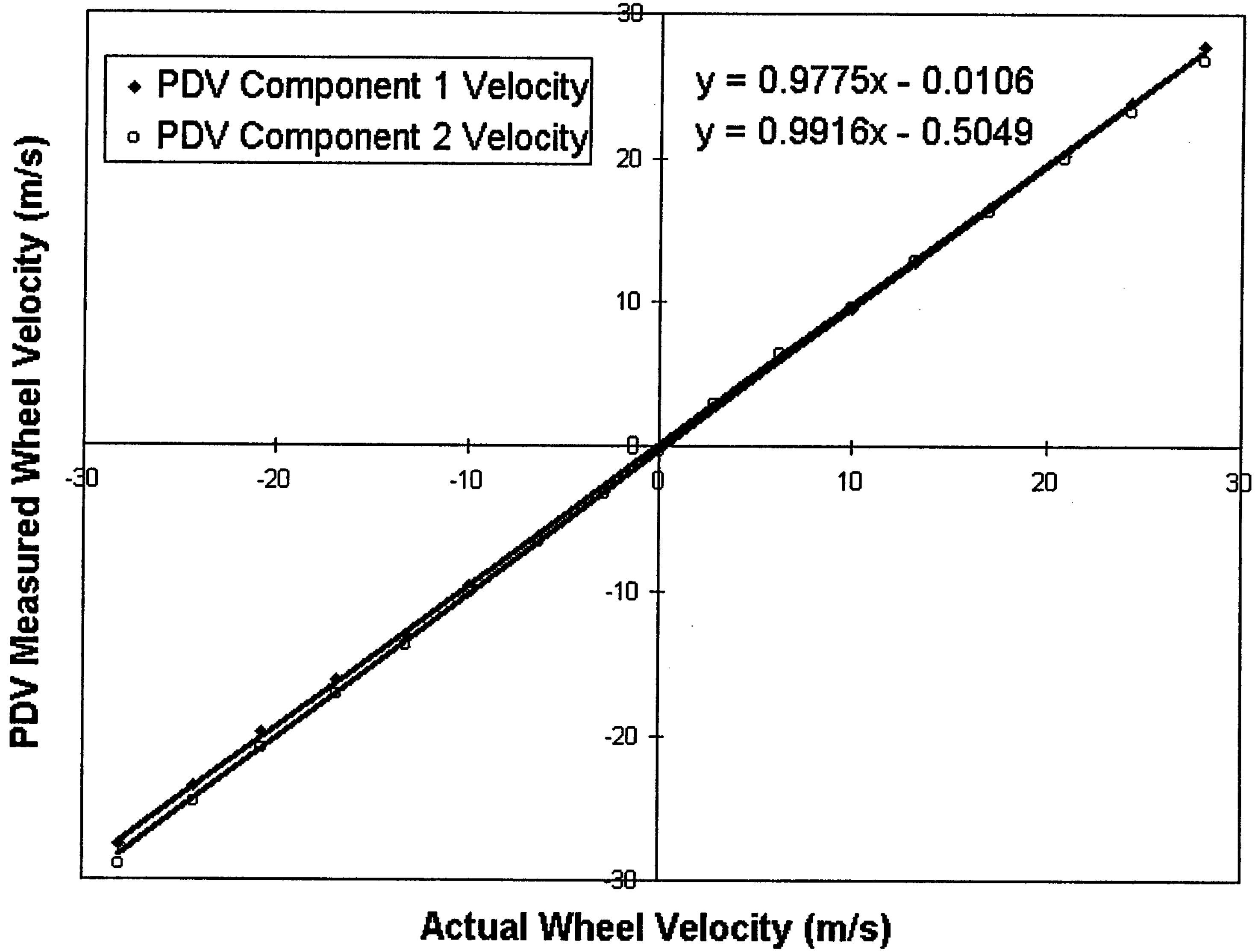

Fig. 12 Two-component PDV data on a rotating wheel showing 0.7% RMS deviation from linear response

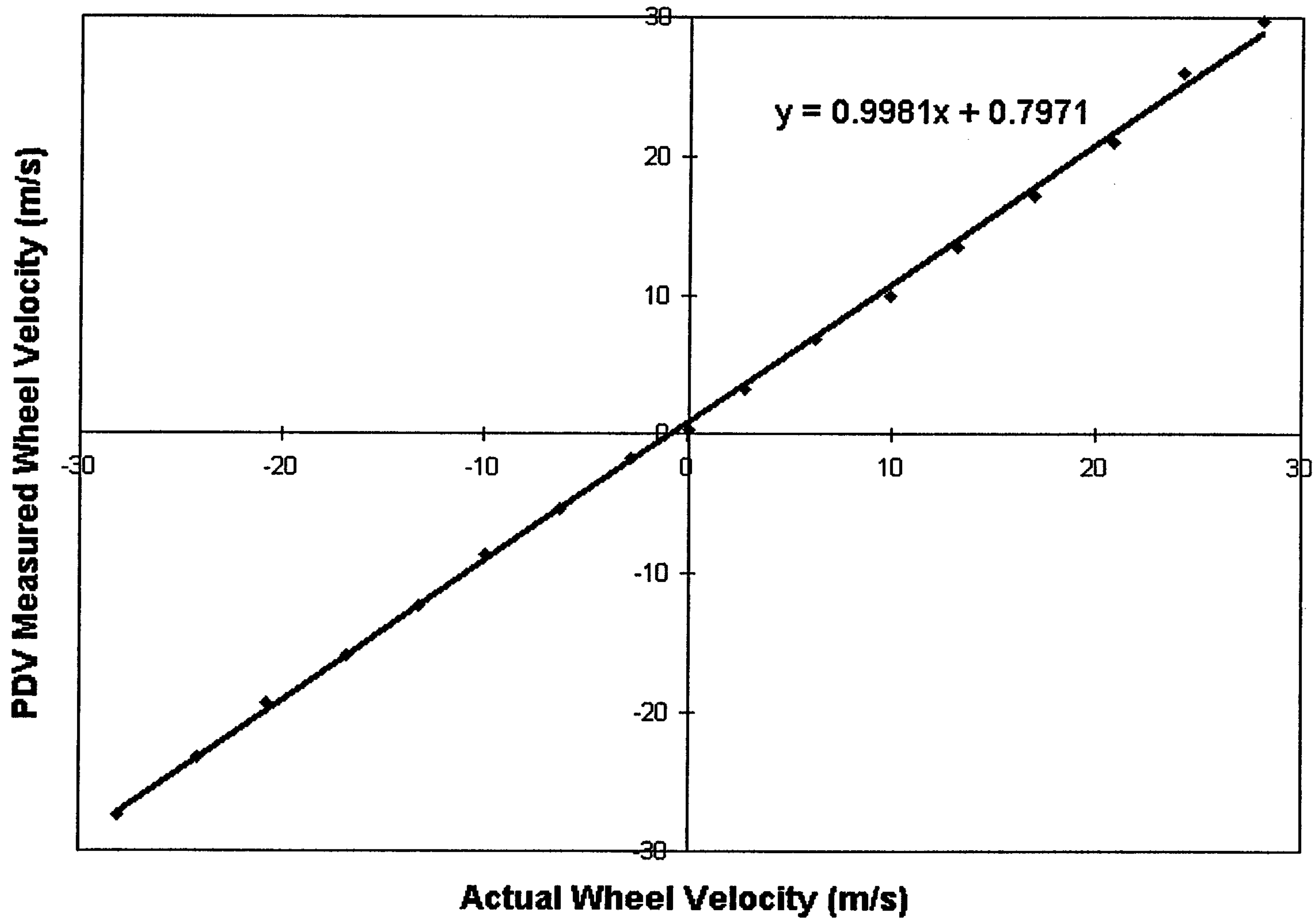

Fig. 13 Typical PDV mean velocity data for rotating wheel: two-component setup

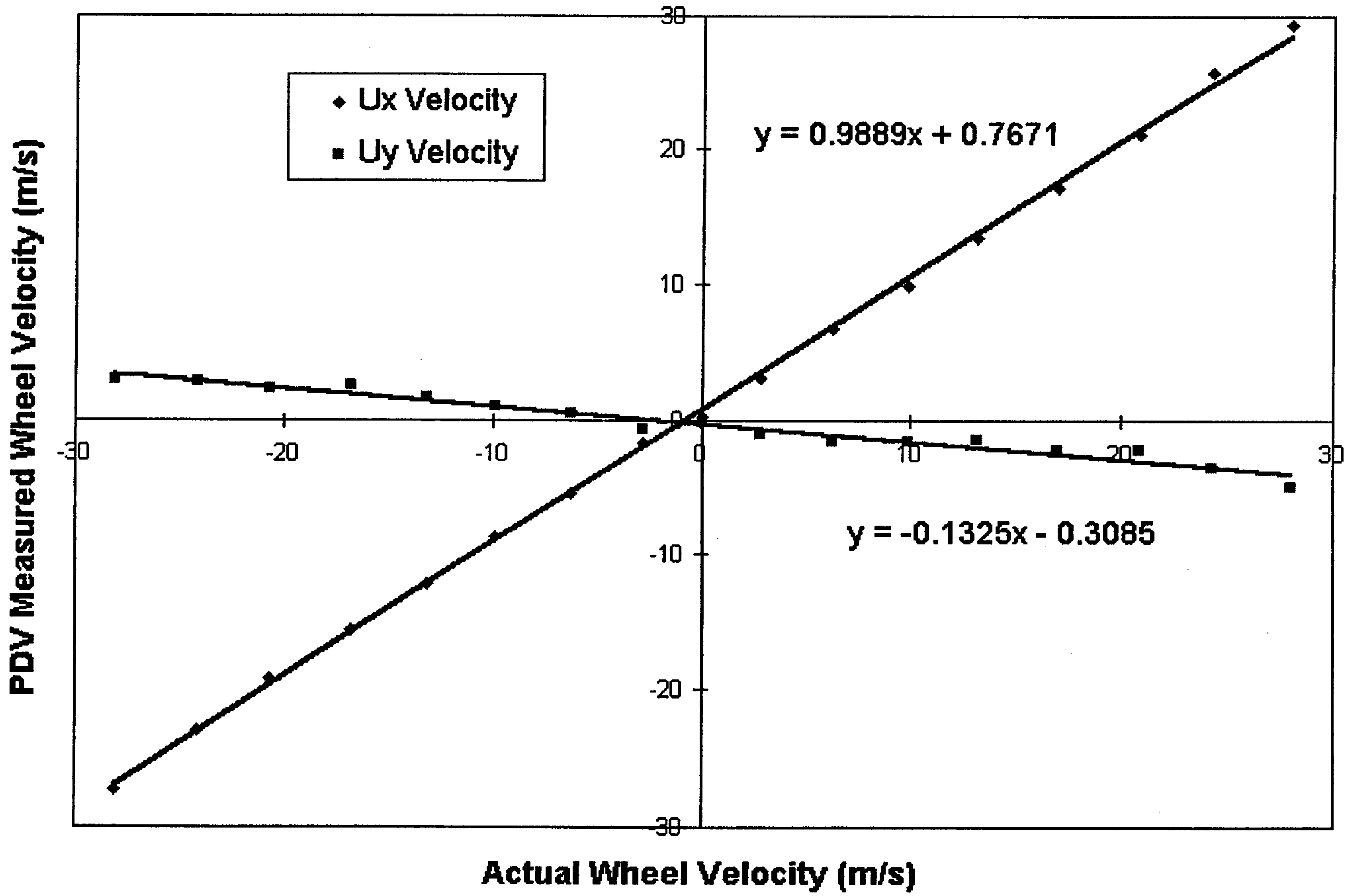

Fig. 14 Measured x- and y-velocity components used to compute wheel velocity magnitude in Fig. 13

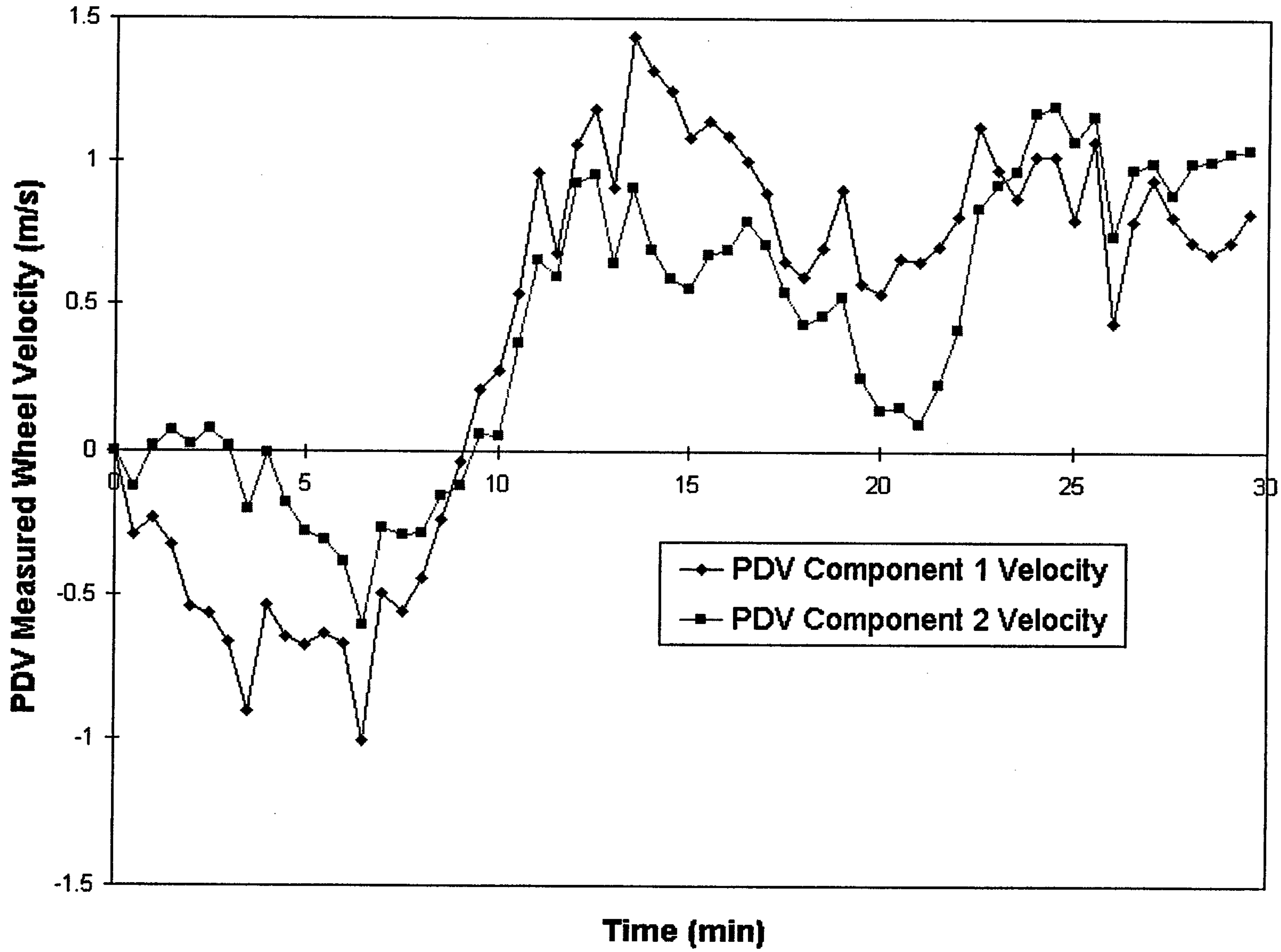

Fig. 15 Measured zero velocity drift over a 30 minute period

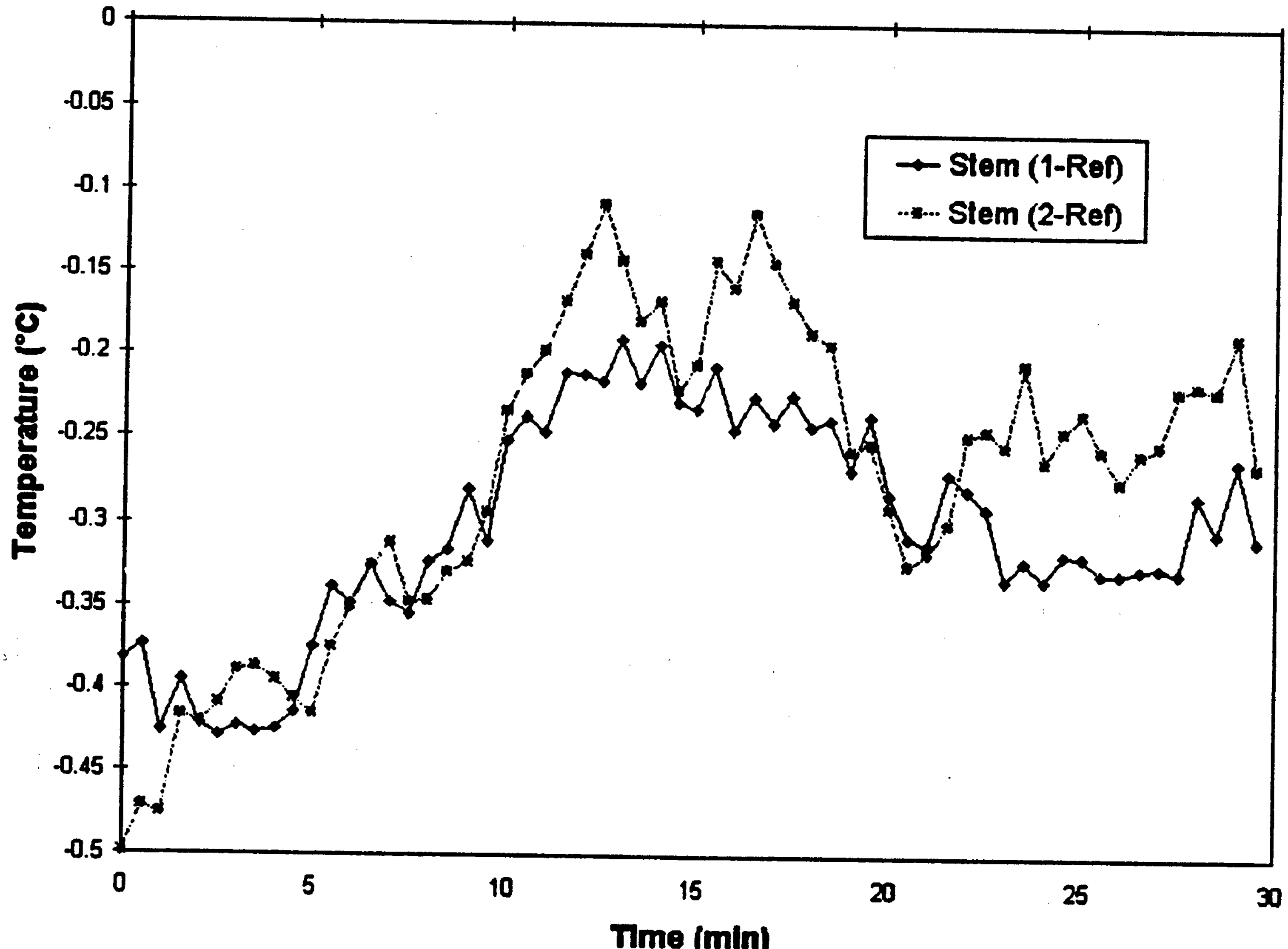

Fig. 16 Differences between signal iodine cell stem temperature and reference cell stem temperature, over same time period as in Fig. 15

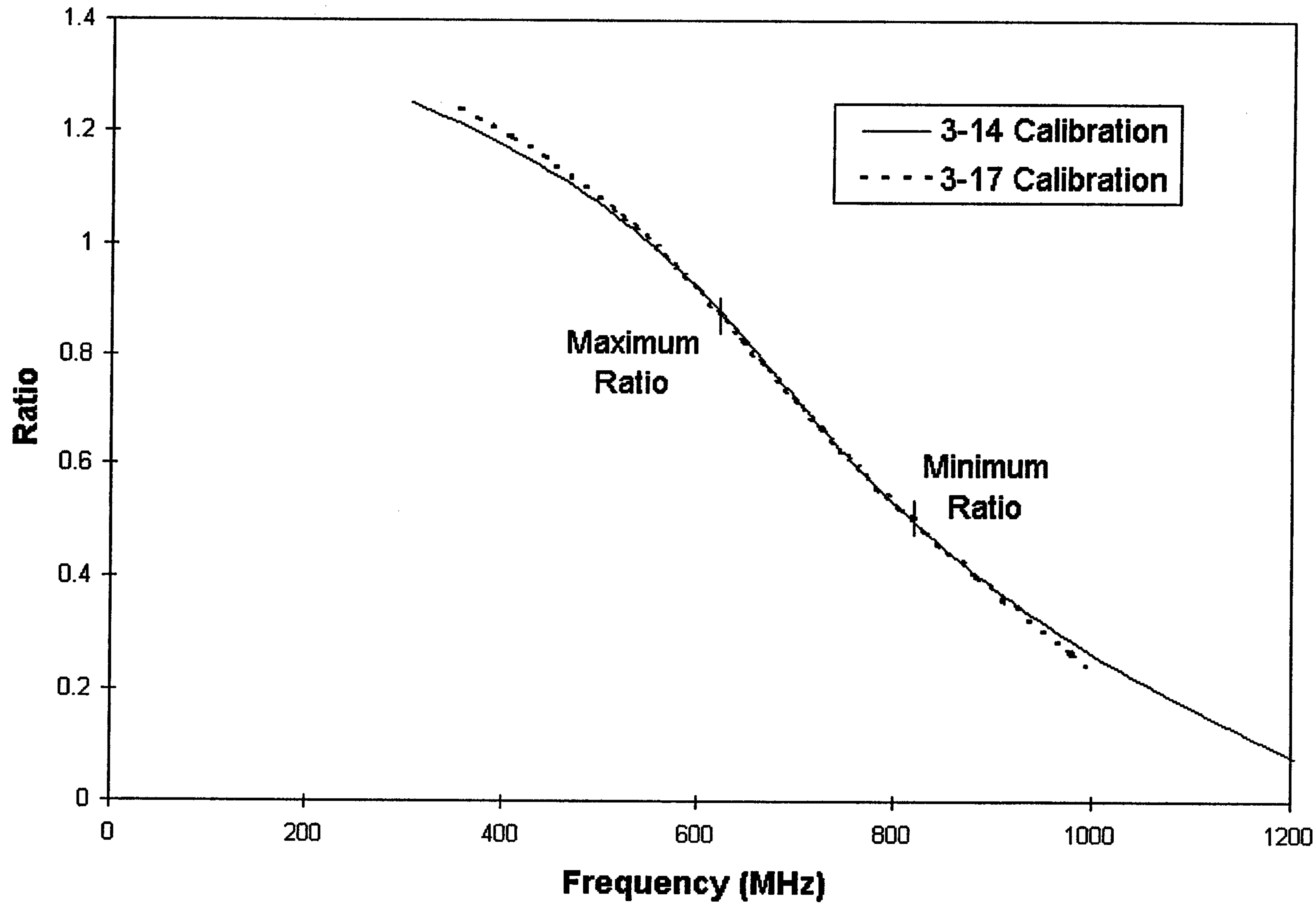

Fig. 17 Repeatability of cell calibration curves, used to estimate velocity error due to calibration

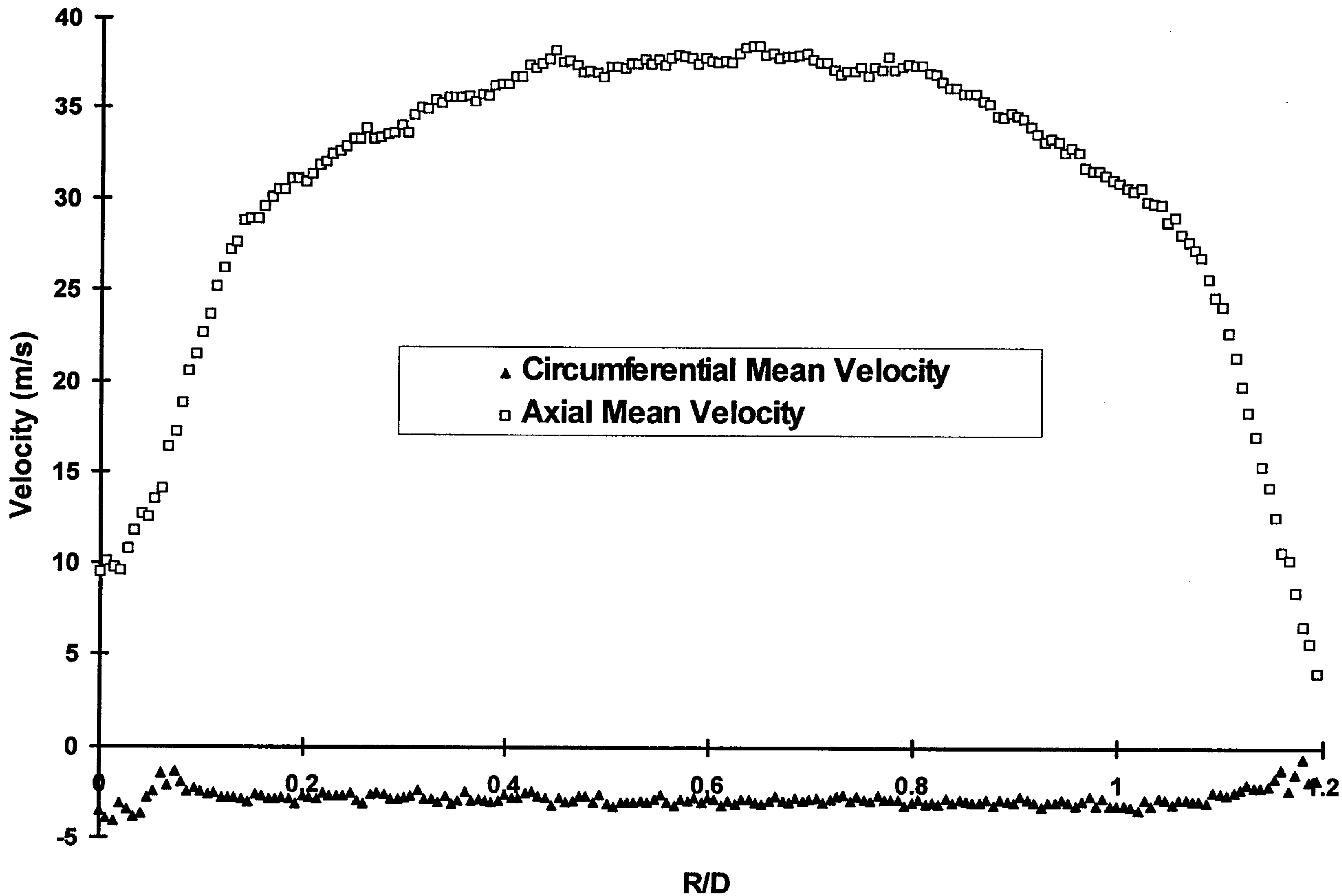

Fig. 18 Two-component PDV mean velocity profiles in 1.5" diameter fully-developed turbulent pipe flow

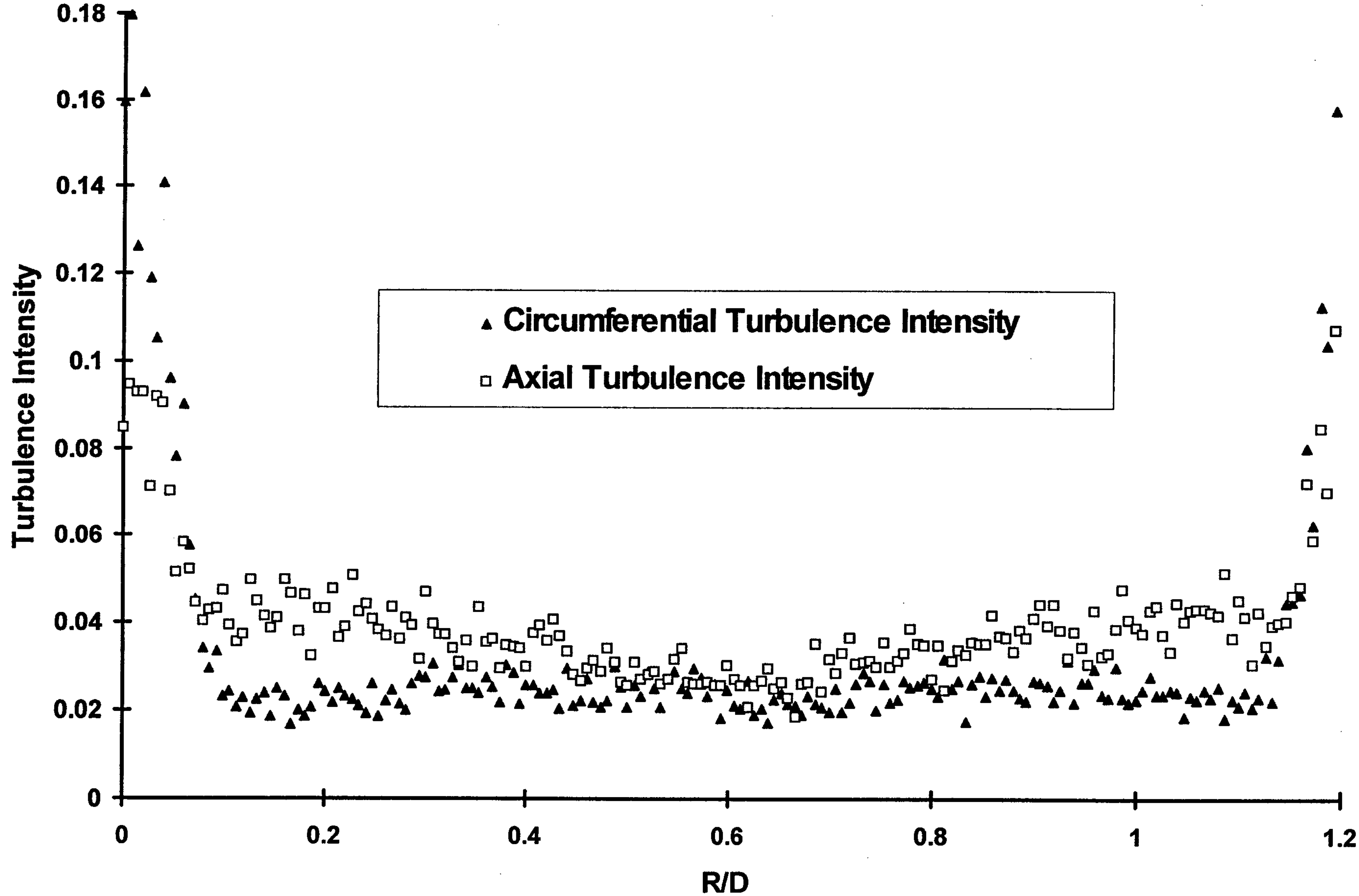

Fig. 19 Two-component PDV turbulence intensity profiles in 1.5" diameter fully-developed turbulent pipe flow

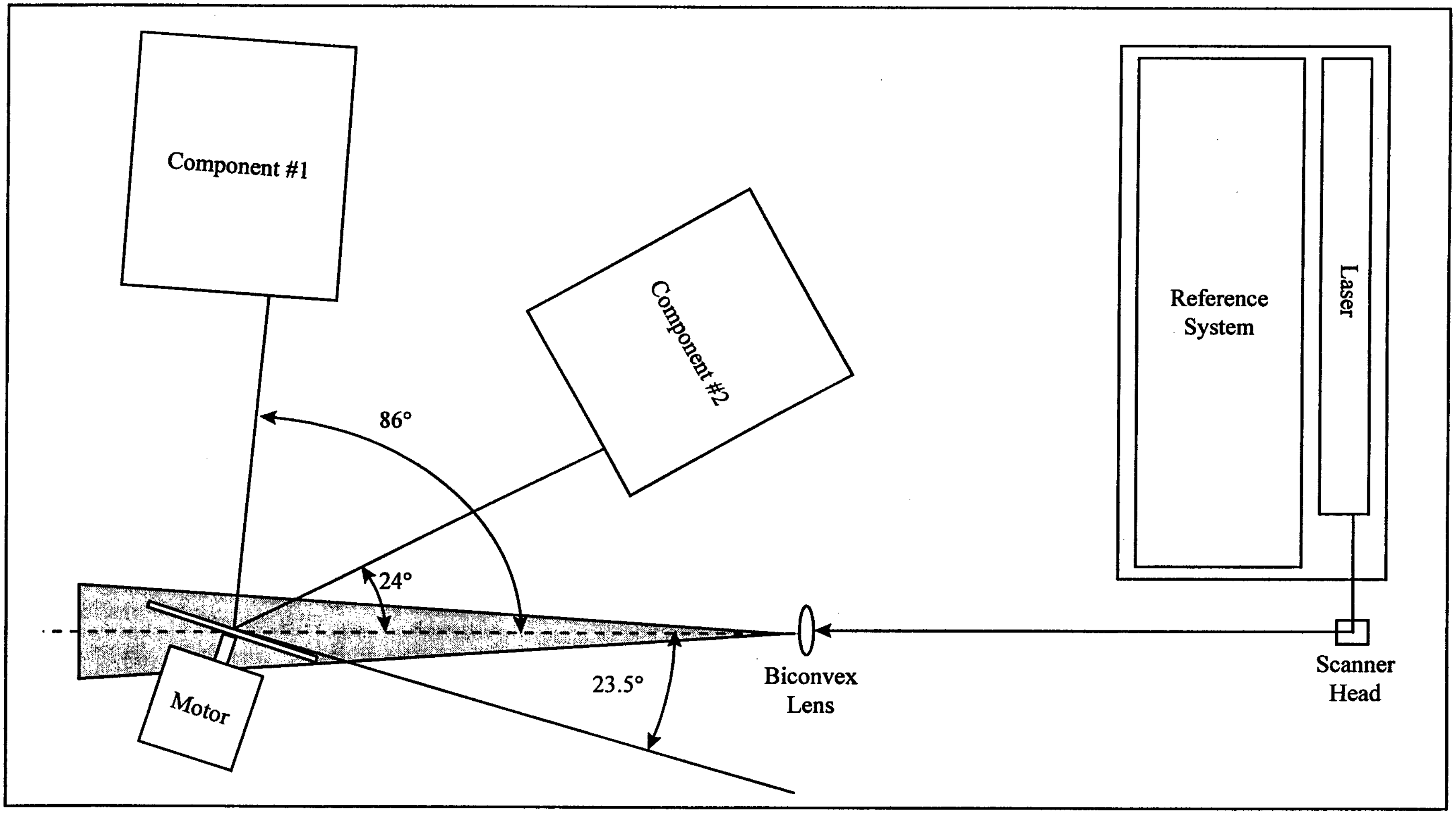

Fig. 20 Top view schematic of DGV system setup for rotating wheel experiment

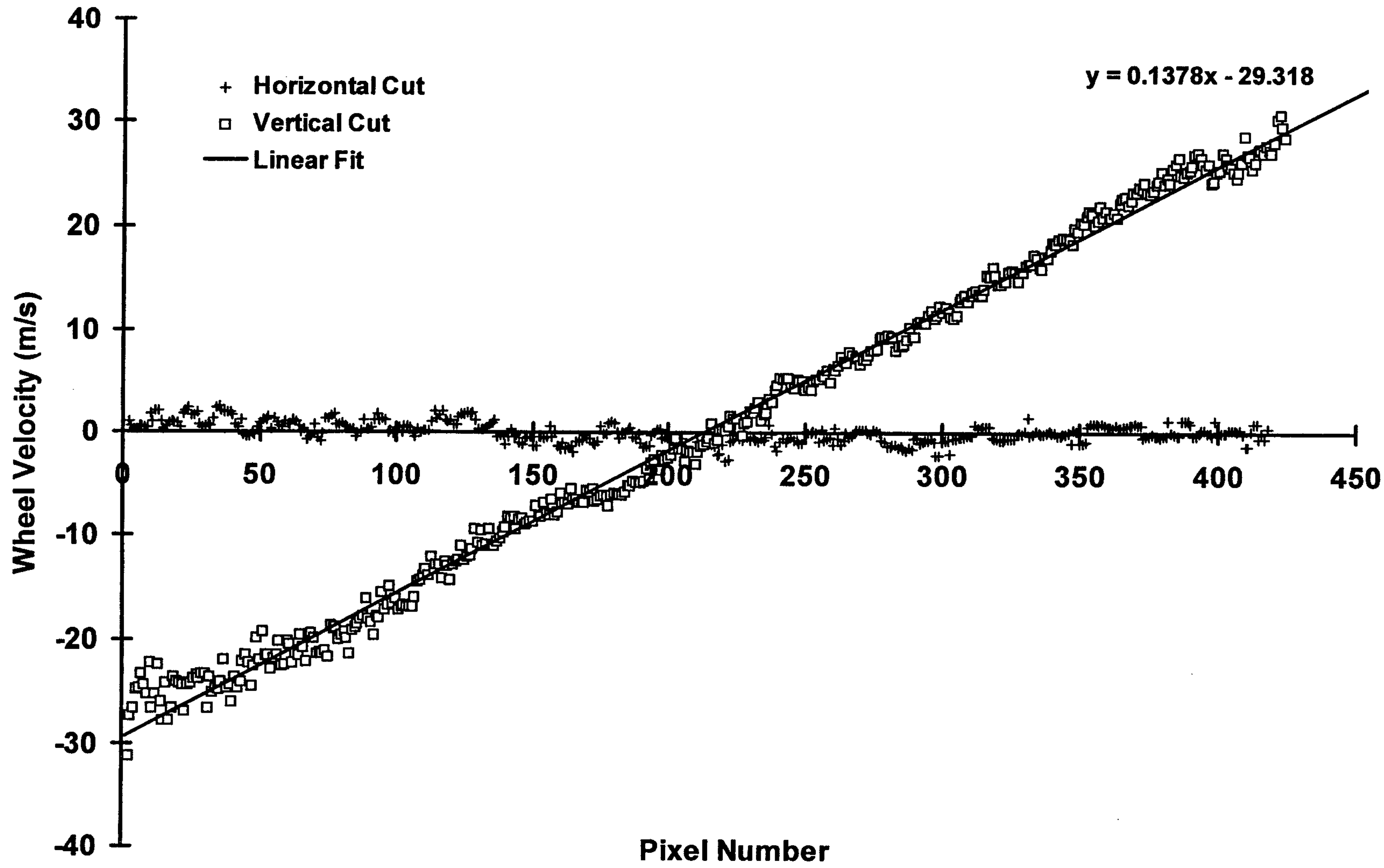

Fig. 21 Horizontal and vertical cuts through an average of 30 DGV velocity images of the surface of a rotating wheel.

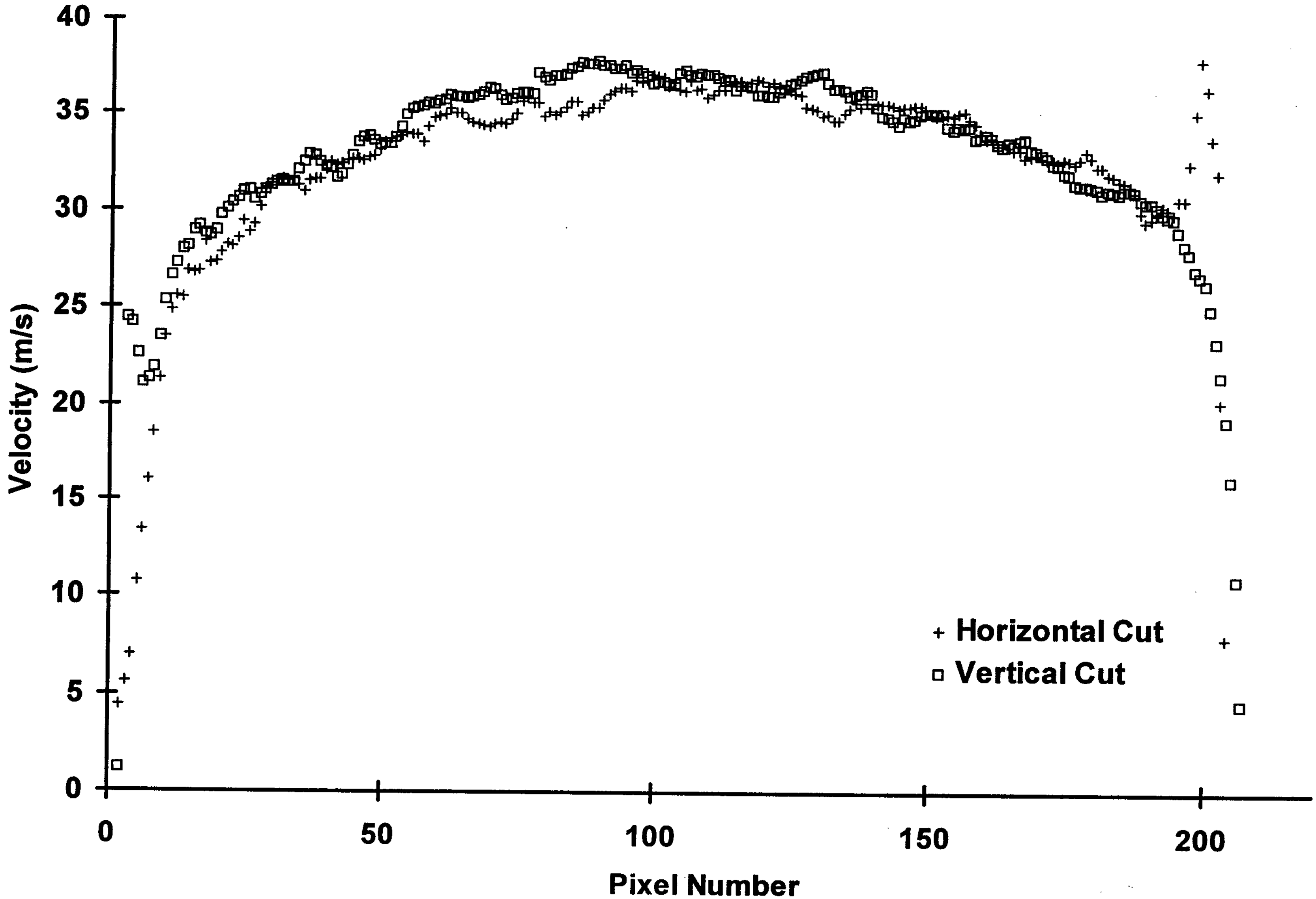

Fig. 22 Horizontal and vertical cuts through an average of 30 DGV velocity images of fully-developed turbulent pipe flow.